Nickel and iron partitioning between clay minerals, Fe-oxides and Fe-sulfides in lagoon sediments from New Caledonia

Pauline Merrot, Farid Juillot, Vincent Noël, Pierre Lefebvre, Jessica Brest, Nicolas Menguy, Jean-Michel Guigner, Marine Blondeau, Eric Viollier, Jean-Michel Fernandez, et al.

▶ **To cite this version:**

Pauline Merrot, Farid Juillot, Vincent Noël, Pierre Lefebvre, Jessica Brest, et al.. Nickel and iron partitioning between clay minerals, Fe-oxides and Fe-sulfides in lagoon sediments from New Caledonia. Science of the Total Environment, 2019, 689, pp.1212-1227. 10.1016/j.scitotenv.2019.06.274 . hal-02343441

HAL Id: hal-02343441
https://hal.science/hal-02343441

Submitted on 16 Nov 2020

HAL is a multi-disciplinary open access archive for the deposit and dissemination of scientific research documents, whether they are published or not. The documents may come from teaching and research institutions in France or abroad, or from public or private research centers.

L'archive ouverte pluridisciplinaire **HAL**, est destinée au dépôt et à la diffusion de documents scientifiques de niveau recherche, publiés ou non, émanant des établissements d'enseignement et de recherche français ou étrangers, des laboratoires publics ou privés.

*Manuscript (double-spaced and continuously LINE and PAGE numbered)-for final publication
Click here to view linked References

Nickel and iron partitioning between clay minerals, Fe-oxides and Fe-sulfides in lagoon sediments from New Caledonia

Pauline Merrot[a], Farid Juillot[a,b], Vincent Noël[c], Pierre Lefebvre[a], Jessica Brest[a], Nicolas Menguy[a], Jean-Michel Guigner[a], Marine Blondeau[a] , Eric Viollier[d], Jean-Michel Fernandez[e], Benjamin Moreton[e], John Bargar[c] and Guillaume Morin[a]

[a] *Institut de Minéralogie, de Physique des Matériaux et de Cosmochimie (IMPMC), UMR 7590 CNRS-SU-IRD-MNHN, Sorbonne Université, case 115, 4 place Jussieu, 75252 Paris Cedex 5, France*

[b] *Institut de Recherche pour le développement (IRD), UMR 206/UMR 7590 IMPMC, 98848 Nouméa, New Caledonia*

[c] *Stanford Synchrotron Radiation Lightsource, SLAC National Accelerator Laboratory, 2575 Sand Hill Road, MS 69, Menlo Park, CA 94025, USA*

[d] *Institut de Physique du Globe de Paris (IPGP), Sorbonne Paris Cité, Univ Paris Diderot, CNRS, F-75005 Paris, France*

[e] *Analytical Environmental Laboratory (AEL), 98800 Nouméa, New Caledonia*

*Graphical Abstract

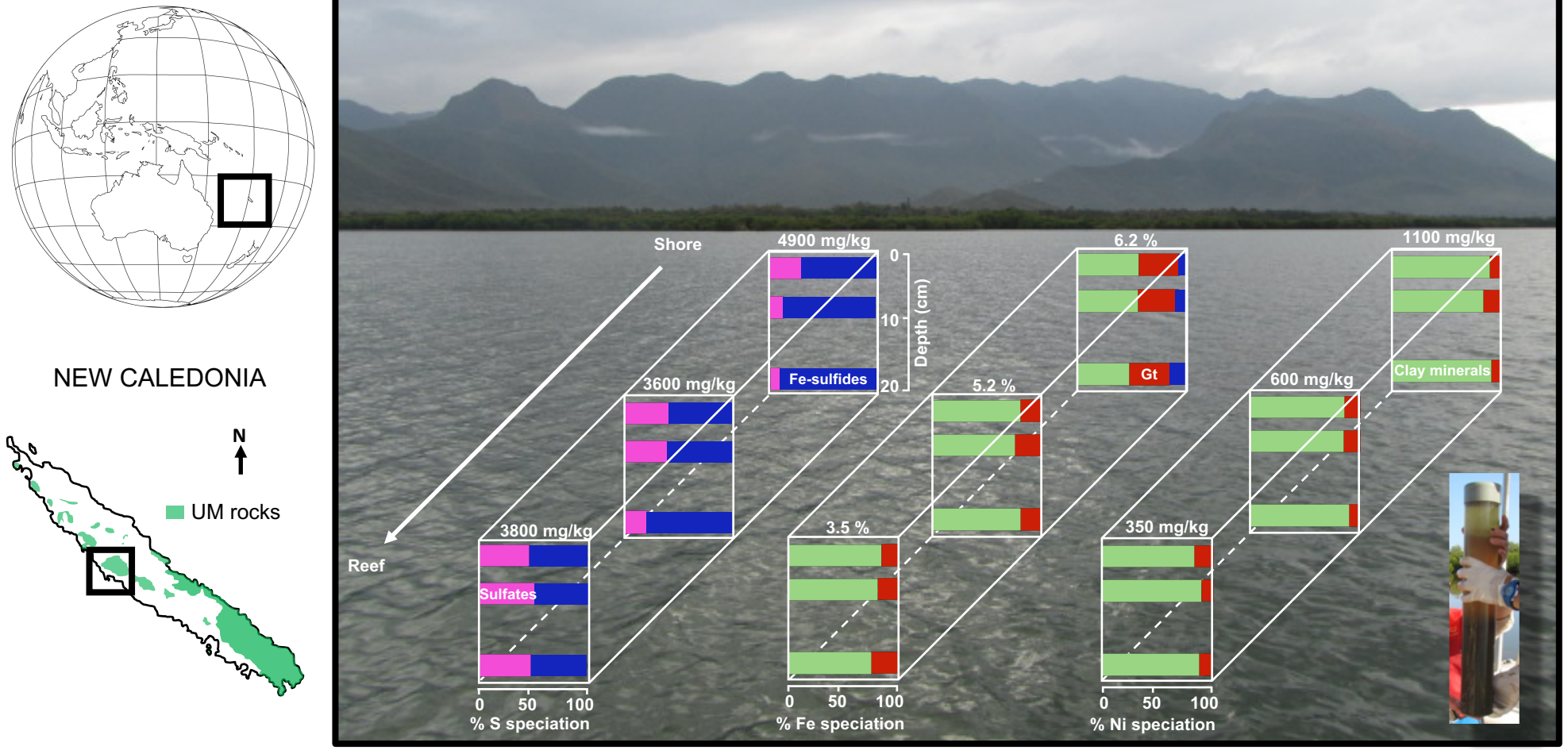

*Highlights (for review : 3 to 5 bullet points (maximum 85 characters including spaces per bullet point)

Highlights

- Pyrite contribution to Ni and Fe speciation is low and restricted to the sediments close to the shore
- Clay minerals are the major host for Fe and Ni across the shore-to-reef gradient
- Fe-rich smectite, glauconite, chrysotile and greenalite/berthierine are the major Fe and Ni-bearing clay minerals identified
- Greenalite/berthierine is the most Ni-rich clay mineral identified and it is considered to have formed *in-situ* upon early diagenesis
- Green clay authigenesis might represent a major process for trace metals cycling in shallow lagoon sedimentary settings

ABSTRACT

In the tropics, continental weathering and erosion are major sources of trace metals towards estuaries and lagoons, where early diagenesis of sediments may influence their mobility and bioavailability. Determining trace metals speciation in tropical sedimentary settings is thus needed to assess their long-term fate and potential threat to fragile coastal ecosystems. In this study, we determined Fe, Ni and S speciation across a shore-to-reef gradient in sediments from the New Caledonia lagoon that receive mixed contribution from lateritic (iron-oxyhydroxides and clay minerals), volcano-sedimentary (silicates) and marine (carbonate) sources. Sulfur K-edge XANES data indicated a major contribution of pyrite (FeS_2) to S speciation close to the shore. However, this contribution was found to dramatically decrease across the shore-to-reef gradient, S mainly occurring as sulfate close to the coral reef. In contrast, Fe and Ni K-edge XANES and EXAFS data indicated a minor contribution of pyrite to Fe and Ni speciation, and this contribution could be evidenced only close to the shore. The major fractions of Fe and Ni across the shore-to-reef gradient were found to occur as Ni- and Fe-bearing clay minerals consisting of smectite (~nontronite), glauconite and two types of serpentines (chrysotile and greenalite/berthierine). Among these clay minerals, greenalite/berthierine, glauconite and possibly smectite, were considered as authigenic. The low contribution of pyrite to trace metals speciation compared to clay minerals is interpreted as a result of (1) a reduced formation rate due to the low amounts of organic carbon compared to the Fe pool and (2) regular re-oxidation events upon re-suspension of the sediments top layers due to the specific context of shallow lagoon waters. This study thus suggests that green clay authigenesis could represent a key process in the biogeochemical cycling of trace metals that are delivered to lagoon ecosystems upon continental erosion and weathering.

KEYWORDS

Lagoon sediments, trace metals, speciation, green clays, TEM, XAS.

1. INTRODUCTION

Thanks to its wet climate, the intertropical zone is the preferential worldwide area for the formation of laterites (Tardy, 1997; Rettalack, 2010). Among these laterites, some have developed upon ultramafic rocks, which represent about 1% of the surface of the earth (Oze et al., 2007). This is for instance the case in Brazil (Raous et al., 2013; Ratie et al., 2018), Cuba (Oliveria et al., 2001), Indonesia (Golightly 1979; Fu et al., 2018), Colombia (Gleeson et al., 2004), Cameroon (Yongue-Fouateu et al., 2006), Australia (Elias et al., 1981) and New Caledonia (Beauvais et al., 2007; Fandeur et al., 2009a; 2009b; Dublet et al., 2012; 2014; 2017). Ultramafic rocks are composed of ferromagnesian minerals (*i.e.* olivine, pyroxene and amphibole), whereas laterites are mainly composed of Fe-(oxyhydr)oxides (*i.e.* mostly goethite FeO(OH), and at a lesser extent hematite Fe_2O_3 and magnetite Fe_3O_4; Oliveria et al. 2001; Yongue-Fouateu et al., 2006; Fandeur et al., 2009a; Raous et al., 2013; Dublet et al., 2012; 2014; 2017; Ratie et al., 2018). Trace metals such as nickel (Ni), chromium (Cr), cobalt (Co) and manganese (Mn) are usually highly concentrated in the Fe-(oxyhydr)oxides of laterites when developed upon ultramafic rocks (Oliveria et al., 2001; Gleeson et al., 2004; Yongue-Fouateu et al., 2006; Fandeur et al., 2009a; Dublet et al., 2012; 2014; 2017; Raous et al., 2013; Fu et al., 2018; Ratie et al., 2018). This is due to their significant concentration in primary ferromagnesian minerals and to their similar crystal-chemistry with Fe(III), which favors their structural incorporation in secondary Fe-(oxyhydr)oxides (Cornell and Schwertmann, 2004). Natural erosion of laterites has thus been responsible for large inputs of trace metals to continental and marine sedimentary settings for million years.

This is especially the case in New Caledonia, where about 30% of the main island surface is covered with laterites that developed several millions of years ago upon ultramafic rocks

(Sevin et al., 2012) and are thus enriched in Fe (~36.93 wt%), Ni (~1.15 wt%), Cr (~1.9 wt%), Co (~0.08 wt%) and Mn (~1.75 wt%) (Fandeur et al., 2009a; 2009b; Dublet et al., 2012; 2017). Since most of these laterites are scattered along the coast and regarding their strong natural erosion due to the tropical climate, shoreline ecosystems of New Caledonia (*i.e.* mangrove and lagoon) have been receiving large amounts of trace metals for million years. Moreover, these inputs are considered to have been significantly enhanced in the last 150 years due to open-cast mining of Ni ores that developed across the main island since the middle of the 19th century. As a consequence, the concentration of trace metals in the mangrove (Marchand et al., 2012; Noël et al., 2014, 2015) and lagoon (Ambatsian et al., 1997; Dalto et al., 2006; Fernandez et al., 2006) sediments of New Caledonia are significantly higher than in other similar environmental settings around the world (Pacifico et al., 2007; Morisson et al., 2010; Lewis et al., 2011; Coates-Marnane et al., 2016; Birch et al., 2017; Saravanan et al., 2018; Zonta et al., 2018).

Once in the sedimentary setting, metals can be involved in many reactions during early diagenesis. Among these numerous reactions, biologically catalyzed reduction of sulfates to sulfides and Fe(III) to Fe(II) in anoxic conditions is known to lead to the formation of Fe-sulfides (*i.e.* mainly pyrite FeS_2, but also mackinawite FeS and greigite Fe_3S_4 which are usually included in the generic term of Acid Volatile Sulfides or AVS) (Morse et al., 1987; Huerta-Diaz et al., 1992; Roberts and Turner 1993; Gagnon et al., 1995; Passier et al., 1996; Butler and Rickard 2000; Rickard and Morse, 2005; Neumann et al., 2005; Alvarez-Iglesias et al., 2012; Botsou et al., 2015). Among Fe-sulfides, pyrite and mackinawite have been extensively investigated for their strong capacity at trapping trace metals, either through analysis of natural sediments or through laboratory-controlled (bio)synthesis experiments (Huerta-Diaz et al., 1992; 1998; 2014; Morse and Luther, 1999; Rickard and Luther, 2007; Burton et al., 2008; Berner et al., 2013; Neumann et al., 2013; Diaz-de-Alba et al., 2016; Le

93 Pape et al., 2016; Ikogou et al., 2017; Morin et al., 2017; Wilkin and Beck, 2017). However,
94 several studies on natural sediments have also shown that trace metals can be associated with
95 silicate minerals and reducible Fe- and Mn-oxides (Lopez-Sanchez et al., 1996; Jones and
96 Turki 1997; Morillo et al., 2004; Yuan et al., 2004; Cuong and Obbard 2006). This is the case
97 in New Caledonia, where some studies reported that Fe-(oxyhydr)oxides and clays are the
98 major host of trace metals (*i.e*. Ni, Cr, Co and Mn) in lagoon sediments (Ambatsian et al.,
99 1997; Fernandez et al., 2006). In contrast, other studies of mangrove sediments from New
100 Caledonia showed that trace metals are sequestered by Fe-sulfides through pyritization
101 (Marchand et al., 2012; 2016; Noël et al., 2014; 2015; 2017). This apparent discrepancy could
102 indicate a different biogeochemical cycling for trace metals in mangrove and lagoon
103 sediments of New Caledonia. However, it could also be due to the fact that the former studies
104 performed on the lagoon sediments relied on sequential chemical extractions that suffer a lack
105 of specificity particularly in anoxic sediments (Jouanneau et al., 1983; Rapin et al., 1986;
106 Nirel and Morel, 1991). Indeed, in their study, Ambatsian et al. (1997) emphasized that
107 carbonates and weakly crystalline oxides could have been dissolved in the first step of their
108 extraction procedure and that a part of weakly crystalline sulfides could have been counted
109 with Mn- and Fe-(hydr)oxides. Therefore, the absence of Fe-sulfides contribution to trace
110 metals speciation reported in this study could be due to a lack of precision of the
111 methodological approach used by these authors. This doubt was not risen by the study of
112 Fernandez et al. (2006), which focused on surface sediment samples and thus did not bring
113 additional information able to describe the crystal-chemistry of trace metals during early
114 diagenesis in the lagoon sediments of New Caledonia.
115 Owing to their potential toxicity to living organisms (Di Toro et al., 1992), this lack of
116 information is an important issue because early diagenesis in the lagoon sediments of New
117 Caledonia could modify the crystal-chemistry of trace metals, and possibly induce some

changes in their mobility and bioavailability that could reveal deleterious for the long term sustainability of this fragile ecosystem. Since Ni is the major trace metal mined in New Caledonia, the objective of the present study was to improve our understanding of the biogeochemical cycling of this element in the lagoon sediments of New Caledonia through a thorough evaluation of its actual speciation along the trace metals input gradient. For that purpose, we selected two lagoon bays located downstream of one of the largest mined lateritic Ni-ores from New Caledonia and sampled three sediment cores under controlled anoxic conditions across a shore-to-reef gradient for each bay. In addition, we also sampled one sediment core downstream of a siliceous non-mined watershed to serve as reference. For each sediment core, we used X-Ray Diffraction (XRD), Scanning Electron Microscopy – Energy Dispersive X-Ray Spectroscopy (SEM-EDXS) analyses, Transmission Electron Microscopy – Energy Dispersive X-Ray Spectroscopy (TEM-EDXS) analyses and synchrotron-derived X-Ray Absorption Spectroscopy (XAS) to identify and quantify the Ni species as a function of depth. Due to their potential strong association with Ni, the speciation of Fe and S were also studied. The results obtained reveal the major trends in the biogeochemical cycling of Ni, but also Fe and S, within the lagoon sediments of New Caledonia downstream lateritic Ni-ores.

2. MATERIALS AND METHODS

2.1 Sampling site and sampling procedures

New Caledonia is located in the South-West Pacific Ocean under oceanic tropical climate (Fig. 1). The main island (Grande Terre) extends over ~500km long and ~50km wide (Fig. 1). It is surrounded by the second largest reef barrier in the world (*i.e.* about 1500 km long) that delineates a lagoon of about 30,000 km^2 (Cabioch et al., 1999; 2003; Andrefouët et al., 2009; Debenay et al., 2009; Anderfouët and Wantiez, 2010; Grenz et al., 2010a; Ouillon et al.,

2010). The two major features of this lagoon setting are the shallow depth of water (*i.e.* rarely more than 50m; Grenz et al., 2010b; Minghelli-Roman and Dupouy, 2013) and its oligotrophic to mesotrophic characteristics (Jacquet et al., 2006; Torreton et al., 2007; 2010; Dupouy et al., 2010; Fichez et al., 2010). The studied site is located on the North-Western part of the lagoon from New Caledonia (Voh-Kone-Pouembout or VKP area, Northern Province; Fig. 1), where about 90% of the water depth is less than 20m (Wattelez et al., 2016). The studied sediment cores were sampled in the Vavouto, Kataviti and Chasseloup Bays in July 2016 during the dry season (Fig. 1). The Vavouto Bay is located downstream of the ultramafic Koniambo outcrop (20°59'S; 164°49'E) composed of deeply weathered peridotites and thus characterized by Ferralsols enriched in Fe, Mn, Cr, Ni and Co (*i.e.* concentrations up to 50-55 wt%, 8-9 wt%, 3-4 wt%, 2.0-2.5 wt% and 0.5-0.6 wt%, respectively; Fandeur et al., 2009a; Dublet et al., 2012; 2017). The Chasseloup Bay is located downstream of a volcano-sedimentary setting mainly composed of Acrisols, Cambisols Vertisols and Fluvisols (Fritsch, 2012) that are characterized by medium to high Si, Al, Mg and K concentrations (*i.e.* up to 40-45 wt%, 7-8 wt%, 4-4.5 wt%, 0.4-0.5 wt%, respectively; Vincent et al., 2018). The Kataviti Bay is located at an intermediate position, downstream of both types of ultramafic and volcano-sedimentary settings (Fig. 1). In both the Vavouto and Kataviti Bays, three sediments cores were collected at an increasing distance across the shore-to-reef gradient : less than 100 m from the mangrove limit (stations referred hereafter as ''close to the shore''), 2-3 km from the mangrove limit (stations referred hereafter as ''intermediate'') and 5-6 km from the mangrove limit (stations referred hereafter as ''close to the coral reef''). Only one sediment core was collected at an intermediate position (about 2 km from the mangrove limit) in the Chasseloup Bay (Fig. 1). Each sediment core was conserved at room temperature with its overlying water no longer than 3 hours. Before sampling, dissolved oxygen concentration in the pore water was determined by inserting a

glass micro-electrode in the sediment at 50 µm steps down to ~10 mm depth. All sediments were found to be anoxic below 2 to 5 mm (Fig. S1). After dissolved oxygen measurements, the sediments were sampled every 1 cm under N_2 flow in order to prevent any oxidation and each sample was immediately stored under anoxic conditions at 4°C in glass vials sealed with a butyl rubber stopper. After about 4 weeks of storage, the samples were opened in a glove box under N_2 atmosphere ($[O_2] \leq 1$ ppm) for vacuum-drying. After drying, each sample was ground in the glove box, with an agate mortar for XRD analyses and with a mechanical grinder at a 30 Hz frequency during 20 min for chemical and spectroscopic analyses. After manual or mechanical grinding, all samples were stored in sealed glass vials and maintained in the glove box until analyses.

2.2 Chemical and mineralogical analyses

Bulk concentrations of major (Ca, Mg, Na, K, Ti, Fe, Al and Si) and trace (Co, Cr, Mn, Ni, Cu, P and Zn) elements in the studied sediment samples were determined by ICP-OES (VARIAN® 730ES ICP optical emission spectrometer) and ICP-MS (PERKIN ELMER® NexION 350x ICP mass spectrometer) respectively after alkaline fusion. Sulfur concentration was also determined by ICP-MS but after a total acid digestion. Total organic C (C_{org}) and N (N_{org}) concentrations were measured using a SERCON Integra analyzer. All these analyses were performed at the ISO 9001 certified Laboratoire des Moyens Analytiques (LAMA) of the Institut de Recherche pour le Developpement (IRD) in Noumea (New Caledonia).

The mineralogical composition of the sediments was determined by XRD with a PANALYTICAL® X'Pert Pro diffractometer equipped with an X'celerator detector and using Co Kα radiation in order to minimize X-ray absorption by Fe. In the N_2-filled glove box, each sample was mixed with ethanol, and deposited on a zero-background silicon plate that was then inserted in an anaerobic sample chamber to avoid any contact with the atmosphere

195 during transport and XRD analyses (Noël et al., 2014). XRD data were collected in the Bragg-
196 Brentano geometry with a continuous collection mode over the 5-80° 2θ range with a 0.033°
197 2θ step, merging two scans of 2h per sample. Quantitative mineralogical analysis was
198 performed by Rietveld refinement of the XRD patterns using the *xnd* code (Berar, 1998), the
199 sum of the weight fractions of the mineral phase being normalized to unity (Snyder and Bish,
200 1989).
201 The clay fraction (<2 µm) of selected samples was collected using a sedimentation procedure
202 based on the Stokes' law, in an anoxic glove box and using O_2-free deionized water. Oriented
203 deposits were prepared by suspending few tens of milligrams of the separated <2µm fraction,
204 dropping a few hundreds of microliters of this suspension on a glass slide and drying under N_2
205 atmosphere in the glove box. XRD data were then collected on the oriented deposits over the
206 3-16° 2θ range with a 0.017° 2θ step after N_2 drying, after heating at 350 and 550°C for 1h
207 and after solvation with ethylene glycol (*i.e.* oriented deposits left for 24h in a sealed
208 desiccator above an ethylene glycol solution). This procedure is classically designed to
209 identify clay minerals on the basis of their swelling and shrinking behavior (Brindley and
210 Brown, 1980).
211 SEM-EDXS observations and analyses were used to obtain qualitative analyses of the Ni host
212 phases at the micron scale. For this purpose, selected sediment samples were deposited on a
213 carbon tape, dried overnight in a N_2-filled glove box, quickly transported to a carbon coating
214 device and then quickly transferred into the SEM vacuum chamber. SEM observations and
215 analyses were performed at 15kV with a 60µm diaphragm with a Field Emission Gun
216 Scanning Electron Microscope (GEMINI ZEISS Ultra 55) equipped with a Bruker EDXS Si-
217 drift detector.
218 TEM-EDXS observations and semi-quantitative analyses were used to characterize individual
219 clay minerals at the nanoscale. For this purpose, a few milligrams of the clay fraction of

selected samples were suspended in absolute ethanol and dispersed in an ultrasonic bath for a few tens of minutes, before being deposited on a holey carbon-coated grid and rapidly transferred into the TEM airlock. TEM observations and semi-quantitative analyses were performed at 200kV with a JEOL 2110F TEM equipped with a JEOL EDXS Si(Li) detector. The concentration of Si, Mg, Fe, Al, Ni and Cr were first semi-quantified as wt% of SiO_2, MgO, FeO, Al_2O_3, NiO and Cr_2O_3, respectively, and then further transformed to atom% in order to derive the structural formulae of the corresponding clay minerals. The precision of this quantification is considered to be ±10% of the stated wt% (oxides) values.

2.3 Statistical analyses

A two-steps exploratory statistical analysis was performed on the chemical composition of the studied sediments in order for better describing our dataset. In the first step, a Principal Component Analysis (PCA) allowed to determine the relationships among the concentrations of major and trace elements and simplify the dataset by reducing the number of variables into major components. In the second step, a Hierarchical Cluster on Principal Components (HCPC) analysis allowed to group the studied sediments as a function of the principal components extracted from the PCA. For this second step of the procedure, a hierarchical clustering was first performed using the Ward's criterion on the selected principal components of the PCA to group the studied samples on the basis of their chemical characteristics. Then a k-means clustering was done to improve the partition of the studied samples derived from the hierarchical clustering. The number of clusters that are delineated on the final factor map (Fig. 2) correspond to the optimal number of clusters that was defined during the hierarchical clustering on the selected principal components of the PCA. This analysis was performed with the R software (R development Core Team 2008), using the

245 "FactoMineR" package, available at the following link: http://CRAN.R-
246 project.org/package=FactoMineR.
247
248 **2.4 X-ray absorption spectroscopy (XAS) data collection**
249
250 XAS data were collected at the S, Fe and Ni K-edge on the same set of 21 sediment samples,
251 selected at three depths in each of the seven cores.
252
253 *2.4.1 XAS data at the S K-edge*
254 Sulfur K-edge X-ray Absorption Near-edge Structure (XANES) data were collected in
255 fluorescence detection mode at room temperature on the wiggler beamline 4-3 at the Stanford
256 Synchrotron Radiation Light Source (SSRL, CA, USA). The energy of the incoming beam
257 was varied with a Si(111) double-crystal monochromator and the fluorescence signal was
258 collected with a SiLi Vortex detector. Energy was calibrated by setting the energy position of
259 the main edge (1s-3p) of the S K-edge of sodium thiosulfate to 2472.02 eV. Bulk sediment
260 samples were loaded into Al sample holders covered with a 4µm thick layer of S-free
261 Parylene window. The sample holders were prepared in a glove box (3% H_2/97% N_2
262 atmosphere) and analyzed in the sample chamber under He flow. Four scans were averaged
263 for each sample.
264
265 *2.4.2 XAS data at the Fe K-edge*
266 Iron K-edge XANES and Extended X-Ray Absorption Fine Structure (EXAFS) data were
267 collected at cryogenic temperature in N_2 liquid cryostat (80-85K) in fluorescence detection
268 mode using a Canberra® high-throughput Ge 30-element on the wiggler beamline 4-1 at
269 SSRL. One sample was analyzed in transmission mode at cryogenic temperature in liquid He
270 cryostat (15-20K) on the bending magnet FAME beamline at the European Synchrotron

Radiation Facility (ESRF, France). At both beamlines, the energy of the incoming X-ray beam was varied with a Si(220) double-crystal monochromator. Energy was calibrated by setting the first inflection point of the Fe K-edge of a simultaneously measured metallic iron foil to 7112 eV (double transmission mode). For these measurements, pressed pellets were prepared in a glove box under N_2 atmosphere after mixing ~12-18 mg sediment sample with ~35 mg cellulose. Sample pellets were mounted on the cryostat sample rod in the glove box and immersed in a liquid N_2 bath before being transferred into the beamline cryostat. Between 2 and 5 scans were necessary to obtain an acceptable signal-to-noise ratio depending on the Fe concentration in the analyzed sample.

2.4.3 XAS data at the Ni K-edge

Nickel K-edge EXAFS data were collected in fluorescence detection mode at cryogenic temperature in liquid He cryostat (15-20K) on the bending magnet SAMBA beamline at synchrotron SOLEIL (France) for the less dilute samples and on the wiggler beamline 9-3 at SSRL for the most dilute ones. At SAMBA, the energy of the incoming beam was varied with a Si(111) double-crystal monochromator and the fluorescence signal was collected with a Vortex detector. At SSRL BL 9-3, we used a Si(220) double-crystal monochromator and a Canberra® high-throughput Ge 100-elements. Energy was calibrated by setting the first inflection point of the Ni K-edge of a simultaneously measured metallic nickel foil to 8333 eV (double transmission mode). For these measurements, finely ground and homogenized pure samples were prepared as pressed pellets in a glove box under N_2 atmosphere and shipped to the synchrotron facilities in anoxic containers. Sample pellets were mounted on the cryostat sample rod in the glove box and immersed in a liquid N_2 bath before being transferred into the beamline cryostat. Depending on the chemical composition of the sample, 1 to 4 Al foils were used together with Soller slits to improve the signal to noise ratio.

Between 3 and 20 scans were necessary to obtain an acceptable signal-to-noise ratio depending on the Ni (and parasitic Fe) concentrations in the analyzed sample.

2.5 X-ray Absorption Spectroscopy (XAS) data analysis

The data collected at SSRL were calibrated and averaged using the SIXPACK code (Webb, 2005), whereas those collected at SOLEIL and ESRF were calibrated and averaged using the ATHENA code (Ravel and Newville, 2005). All the data were then analyzed by principal component analysis (PCA) using the SIXPACK code (Webb, 2005). The minimum number of principal components necessary to fit each set of sediment samples spectra was chosen on the basis of the minimum value of the factor indicator function (Malinowski 1978, 1987, 1991; Webb, 2005) and of the quality of the reconstruction with up to the four first principal components. Target Transformation (TT) was then used to select the model compounds spectra that we further used in the linear combination least-square fitting (LC-LSF) of the sediment spectra. We used the ATHENA software (Ravel and Newville, 2005) for the LC-LSF analysis of the XANES data and a home-built software based on Levenberg-Marquardt minimization algorithm for the LC-LSF analysis of the EXAFS data (Noël et al., 2014; 2015; Morin et al., 2017).

2.6 Model compounds for XAS analyses

Our database for S K-edge model compounds included a large set of sulfates (SO_4^{2-}) as anhydrite [$CaSO_4$], arcanite [K_2SO_4] (Janot et al., 2016), melanterite [$FeSO_4.7H_2O$], quenstedite [$Fe_2(SO_4)_3.11H_2O$], jarosite [$KFe^{3+}_3(OH)_6(SO_4)_2$] (Kumar et al., 2018), and sulfate organic as Taurine (personal data); thiosulfate ($S_2O_3^{2-}$) as sodium thiosulfate [$Na_2S_2O_3$] (Janot et al., 2016); sulfite (SO_3^{2-}) as [Na_2SO_3] (Kumar et al., 2018); elemental

sulfur (S^0) as polysulfides [S_8] (Janot et al., 2016; Kumar et al., 2018); sulfide (S_2^{2-}) as pyrite and marcasite [FeS_2] (Kumar et al., 2018), synthetic mackinawite [FeS], mackinawite exposed to sub-stoichiometric amounts of weak oxidants or Fe^{3+} referred to as oxidized mackinawite (Noël et al., 2017), pyrrhotite, and greigite [Fe_3S_4] (Kumar et al., 2018).

Our database for Fe K-edge model compounds spectra included a large set of already published data, including Fe(III) (oxyhydr)oxides as goethite [α-FeOOH], hematite [α-Fe2O3], 2-Line, 6-Line ferrihydrite [$Fe^{3+}_2O_3.0.5(H_2O)$] (Maillot et al., 2011; Hohmann et al., 2011), Fe(II)-sulfides as pyrite [FeS_2] and mackinawite [FeS] (Noël et al., 2014) and Fe(II)- and Fe(III)-bearing talc [$(Mg,Fe)_3Si_4O_{10}(OH)_2$] (Stetten et al.,, 2018). It also included natural clay minerals such as illite [$(K,Na,Ca)_x(Al,Fe,Mg)_2(Si,Al)_4O_{10}(OH)_2$] from Le Puy-en-Velay, France (Ildefonse et al., 1998), biotite [$K(Mg,Fe)_3Si_3AlO_{10}(OH)_2$] from Yosemite (Mineralogy Collection of IMPMC, Paris, France) and Garfield nontronite [$Ca_xFe_2(Si,Al)_4O_{10}(OH)_2.nH_2O$] (Washington, USA) (Bonnin et al., 1985).

Our database for Ni K-edge model compounds spectra included a large set of already published synthetic and natural compounds data such as Ni-goethite, Ni-sorbed goethite [α-(Fe,Ni)OOH], Ni-asbolane [$Mn(O,OH)_2Ni_x(OH)_{2x}.nH_2O$] Ni-sorbed birnessite [$(Na,Ca)_{0.5}(Mn,Ni)_2O_4.1.5H_2O$], Ni-serpentine [$(Mg,Fe,Ni)_3Si_2O_5(OH)_4$], Ni-talc [$(Mg,Fe,Ni)_3Si_4O_{10}(OH)_2$] and Ni-montmorillonite [$Ca_x(Al,Mg,Ni)_2Si_4O_{10}(OH)_2.nH_2O$] (Dublet et al., 2012, 2014; Noël et al., 2015).

3. RESULTS

3.1 Bulk chemical composition of the lagoon sediments

Despite few exceptions (Ni, Fe and Co at the KTV station and Ni, Fe and Cr at the VE2 station), trace metals (Ni, Cr, Mn, Co, Ti, Zn and Cu) and major elements (Fe, Si, Al, K, Mg

348 and Ca) concentrations remain quite stable with depth in all sediments cores (Table S1; Figs.
349 S2, S3 and S4). As a consequence, mean concentrations for each core were used to compare
350 the chemical trends from one bay to the other, but also across the shore-to-reef gradient for
351 the Vavouto and Kataviti Bays.
352
353 Comparison of the mean concentrations of elements from one bay to the other allowed to
354 evidence four different chemical trends (Table 1). The first chemical trend is that of mean Ni
355 concentrations that increase from 255±30 $mg.kg^{-1}$ in the Chasseloup Bay (ST16) to 1505±391
356 $mg.kg^{-1}$ close to the shore in the Kataviti Bay (KTV). These concentrations are consistent with
357 those already reported for other parts of the New Caledonia lagoon downstream of lateritic
358 outcrops (Ambatsian et al., 1997; Dalto et al., 2006). They are significantly higher than those
359 reported for tropical lagoon sediments worldwide (1-67 $mg.kg^{-1}$) (Morrison et al., 2010), even
360 at the ST16 station (Chasseloup Bay) which shows the lowest Ni concentrations. Magnesium,
361 Zn and Cu also follow this first chemical trend with mean concentrations that increase from
362 1.67±0.07 wt% (Mg), 63±11 $mg.kg^{-1}$ (Zn) and 26±4 $mg.kg^{-1}$ (Cu) in the Chasseloup Bay
363 (ST16) to 2.26±0.10 wt% (Mg), 86±6 $mg.kg^{-1}$ (Zn) and 38±3 $mg.kg^{-1}$ (Cu) close to the shore
364 in the Kataviti Bay (KTV). The second chemical trend is that of Fe concentrations that
365 increase from 2.67±0.12 wt% close to the reef in the Vavouto Bay (LG2B) to 7.10±0.57 wt%
366 close to the shore in the Kataviti Bay (KTV). As for Ni, these concentrations are consistent
367 with those reported for other parts of the New Caledonian lagoon downstream of lateritic
368 outcrops (*i.e.* 4.5-9.0 wt%; Ambatsian et al., 1997). Titanium, Cr, Mn and Co also follow this
369 second chemical trend with mean concentrations that increase from 1312±82 $mg.kg^{-1}$ (Ti),
370 278±24 $mg.kg^{-1}$ (Cr), 335±20 $mg.kg^{-1}$ (Mn) and 29±14 $mg.kg^{-1}$ (Co) close to the reef in the
371 Vavouto Bay (LG2B) to 4251±169 $mg.kg^{-1}$ (Ti), 2879±378 $mg.kg^{-1}$ (Cr), 85±46 $mg.kg^{-1}$ (Co)
372 and 547±42 $mg.kg^{-1}$ (Mn) close to the shore in the Kataviti Bay (KTV). With higher

concentrations in the Chasseloup Bay, Si, Al and K follow a third chemical trend. Mean concentrations of these elements increase from 8.26±0.75 wt% (Si), 1.76±0.11 (Al) wt% and 0.31±0.02 wt% (K) close to the reef in the Vavouto Bay (LG2B) to 32.47±1.02 wt% (Si), 6.18±0.42 wt% (Al) and 1.15±0.13 wt% (K) in the Chasseloup Bay (ST16). Finally, with mean concentrations that increase from 1.01±0.13 wt% $mg.kg^{-1}$ in the Chasseloup Bay (ST16) to 29.57±0.97 wt% close to the reef in the Vavouto Bay (LG2B), Ca follows a fourth chemical trend.

Comparison of the mean concentrations of elements across the shore-to-reef gradient for both the Vavouto and Kataviti Bays, allowed to depict two opposite trends (Table 1). The first one is that of major elements (Fe, K, Mg, Si and Al), trace metals (Ni, Cr, Mn, Co, Ti, Zn and Cu) and C_{org} and N_{org} concentrations, which show a decrease from the shore to the reef (*i.e.* from KTV to KL2 and from VE2 to LG2B). The second one is that of Ca concentration, which shows an increase from the shore to the reef. These opposite trends are in agreement with the supposed increasing influence of the marine contribution (*i.e.* at the expense of the detrital continental contribution) across the shore-to-reef gradient.

3.2 Statistical assessment of the sediments sources

The results of the PCA performed on the major elements and trace metals concentrations in the studied sediments show that the two first principal components explain 80.69% of the cumulative variance (*i.e.* 59.01% for factor 1 and 21.68% for factor 2; Fig. 2). These results allow to evidence a first clustering for Ni, Mg, Cr, Mn and Co loadings, a second one for K, N_{org}, C_{org}, Ti, Al and Si loadings and a third one for Ca loading (Fig. 2). Iron, Zn, Cu and Na show mixed loadings between both clusters 1 and 2. These three clusters are considered to represent the three major sources to the studied sediments. Due to the large amounts of Ni, Cr, Co, Mn and Mg in the Koniambo outcrop (Fandeur et al., 2009a; 2009b; Dublet et al., 2012;

399 2014), the first cluster is considered to represent the ultramafic/lateritic source to the studied
400 sediments. The results of the HCPC analysis indicate that the two stations located close to the
401 shore downstream of the Koniambo outcrop (KTV and VE2) are the most exposed to this
402 source (Fig. 2). The major and trace elements that are related to the second cluster (*i.e.* K,
403 N_{org}, C_{org}, Ti, Al and Si) are characteristic of the soils developed upon the volcano-
404 sedimentary setting that can be found around the ultramafic Koniambo outcrop (Fig. 1;
405 Houles et al., 2018; Vincent et al., 2018). The second cluster is thus considered to represent
406 the volcano-sedimentary source to the studied sediments and the results of the HCPC analysis
407 show that the reference station (ST16) is the most exposed to this source (Fig. 2). With Ca as
408 the only characteristic element, the third cluster is considered to represent the marine source
409 to the studied sediments and the results of the HCPC analysis indicate that the WR2 and
410 LG2B stations in the Vavouto Bay (Fig. 1) are the most exposed to this source (Fig. 2).
411 Finally, the results of the coupled PCA/HCPC analysis also indicate that the KL1 and KL2
412 stations in the Kataviti Bay (Fig. 1) are exposed to the three sources in roughly similar
413 amounts (Fig. 2).
414
415 **3.3 Mineralogy and crystal-chemistry of the lagoon sediments**
416
417 Quantitative mineralogical analysis (Fig. 3; Table S3) fully confirmed the trends observed in
418 the chemical compositions of the sediments (*i.e.* the increase in the carbonate minerals
419 contribution from the shore to the reef for the Kataviti and the Vavouto Bays, and the larger
420 carbonate minerals contribution in the Vavouto Bay). Indeed, XRD data (Figs. S5, S6 and S7)
421 and their Rietveld refinement (Figs. S8, S9 and S10; Table S3) indicate that the sediments
422 close to the shore, (*i.e.* KTV Figs. S5 and S8, VE2 Figs. S6 and S9 and ST16 Figs. S7 and
423 S10), mainly consist of quartz [SiO_2], albite [$NaAlSi_3O_8$] and muscovite

424 [$KAl_2Si_3AlO_{10}(OH)_2$] / illite [$K_{1-x}Al_{1-x}Si_{3+x}AlO_{10}(OH)_2$] / smectite
425 [$(Na,Ca)_{0.3}(Al,Mg,Fe)_2(Si,Al)_4O_{10}(OH)_2 \bullet nH_2O$]. The muscovite/illite/smectite mixture is
426 considered as a single pool in our Rietveld refinement analysis because of the overlaping
427 contributions of the (*hkl*) Bragg reflections of theses clay minerals to the XRD pattern in the
428 23 – 30° 2θ range, especially the (111) reflection at ~4.35 Å. Small amounts of pyrite [FeS_2]
429 and halite [NaCl] could also be detected in some of the studied samples (Fig. 3). In the same
430 way, minor amounts of two types of serpentines (*i.e.* XRD peak at 7.3 and 7.1 Å) could also
431 be detected. These two latter clay minerals were interpreted as chrysotile
432 [$(Mg,Fe)_3Si_2O_5(OH)_4$] and greenalite [$Fe_3Si_2O_5(OH)_4$]/ berthierine [$(Fe,Al)_3(Si,Al)_2O_5(OH)_4$],
433 respectively, on the basis of TEM-EDXS analyses (see further details below).
434 In contrast, the sediments close to the coral reef (*i.e.* KL2 Figs. S5 and S8 and LG2B Figs. S6
435 and S9) mainly consist of aragonite [$CaCO_3$], magnesian calcite [$(Mg,Ca)CO_3$] and calcite
436 [$CaCO_3$], together with minor amounts of the silicate minerals observed in the sediments
437 close to the shore (Fig. 3). Finally, the sediments sampled at intermediate locations (*i.e.* KL1
438 Figs. S5 and S8 and WR2 Figs. S6 and S9) exhibit a mixed mineralogical composition. For all
439 studied sediments, the mineralogy did not show significant changes with depth (Figs. S5, S6
440 and S7).
441 The XRD patterns obtained on oriented deposits of the clay fraction from the top (0-1 cm) and
442 bottom (20.5-21.5 cm) samples of the VE2 station are displayed in Figure S11. These XRD
443 patterns show major contributions of the basal reflections of swelling smectite (d=15.3Å after
444 air-drying, d=17.1Å after ethylene-glycol solvation) and muscovite/illite (d=10.0 Å), which is
445 consistent with our Rietveld analysis. The XRD peaks at d=7.3 and 7.1 Å are interpreted as
446 the basal reflections of chrysotile and greenalite/berthierine, in agreement with our Rietveld
447 analysis of the XRD powder patterns and with TEM-EDXS results detailed below. Minor
448 amounts of chlorite (d=14.2 Å) are also considered due to the small remaining XRD peak at

449 *d*=7.3 Å after heating to 550°C. In addition, the small basal reflections at 9.5 and 9.3Å
450 suggest the occurrence of minor amounts of Mg- and Fe-rich talc, respectively. The lack of
451 detection of these latter clay minerals in the powder XRD pattern is likely due to their low
452 concentration.
453 SEM-EDXS analyses of selected samples from the VE2 and WR2 stations (Vavouto Bay), as
454 well as from the KTV station (Kataviti Bay), indicate that Ni is mainly associated with
455 mineral aggregates having compositions consistent with those of Fe-rich clay minerals (Fig.
456 S12a) or Fe-(oxyhydr)oxides (Fig. S12b). At a lesser extent, Ni can also be found associated
457 with framboidal pyrite (Fig. S12c), but most of the pyrites analyzed were devoid of Ni (Fig.
458 S12d).
459 TEM analyses of the clay fractions from selected samples from the VE2 and WR2 stations
460 (Vavouto Bay) show 3 types of clay minerals (Fig. 4). The first type exhibits a fibrous and
461 tubular morphology characteristic of chrysotile, and the Mg-rich composition (with minor
462 amounts of Fe) depicted in a Mg-Si+Al-Fe ternary diagram (Fig. 4; Table 2) is consistent with
463 this clay mineral (Table S4). TEM-EDXS analyses indicate that this first clay mineral
464 systematically contains minor amounts of Ni and Cr (0.10 wt% NiO and 0.61 wt% Cr_2O_3, on
465 average; Table 2). The second type of clay minerals appears as massive oriented aggregates of
466 elongated thin layers with a Fe-rich composition (and minor amounts of Al and Mg; Fig. 4;
467 Table 2), which is consistent with the 1/1 stoichiometry of greenalite and berthierine (Table
468 S4). TEM-EDXS analyses indicate greenalite as the most enriched in Ni (6,77 wt% NiO and
469 0.90 wt% Cr_2O_3, on average; Table 2) and berthierine as the most enriched in Cr (1.00 wt%
470 NiO and 1.40 wt% Cr_2O_3, on average; Table 2). Finally, the third type of clay minerals
471 appears as aggregates of nano-sized platelets enriched in Fe and Al (with minor amounts of
472 Mg) and with a 2/1 stoichiometry that is consistent with glauconite and Fe-rich smectite (Fig.
473 4; Table 2). TEM-EDXS analyses of this third type of clay minerals indicate Ni and Cr

concentrations (0.81 wt% NiO and 0.96 wt% Cr_2O_3, on average; Table 2) between those found in chrysotile and those found in greenalite/berthierine.

3.3 XAS analysis of the S, Fe and Ni speciation

A coupled PCA and TT analysis was performed on the S K-edge XANES spectra, Fe K-edge EXFAS spectra and Ni K-edge EXAFS spectra from the 21 studied sediments and a large set of model compounds in order to select the most relevant model compounds for the LC-LSF analysis of experimental data.

The results of the coupled PCA and TT analysis on the S K-edge XANES data indicate anhydrite, pyrite and mackinawite as the most relevant model compounds (Table S5; Fig S13 and 14) to account for the S species in the studied sediments (Table S6; Fig. S15). Anhydrite is here considered as a proxy for sulfate mineral phases in the studied sediments. The results of the LC-LSF analysis of the S K-edge XANES spectra indicate the occurrence of S(VI) represented by sulfate species, S(-I) represented by mackinawite (FeS) and S(-II) represented by pyrite (FeS_2; Figs. 5 and S15). The fraction of sulfide species (*i.e.* pyrite and mackinawite) increases in all sediments, but those collected close to the reef in the Kataviti Bay (KL2; Fig. S15; Table S6). In both the Vavouto and the Kataviti Bays, this proportion decreases from the shore to the reef (*i.e.* from a mean value of 94% at the VE2 station to a mean value of 36% at the LG2B station in the Vavouto Bay and from a mean value of 80% at the KTV station to a mean value of 41% at the KL2 station in the Kataviti Bay; Figs. 5 and S15; Table S6). The mean fractions of sulfides (80%) and sulfates (23%) at the reference station (ST16) in the Chasseloup Bay are similar to those found close to the shore in the Kataviti Bay (KTV) (Figs. 5 and S15; Table S6).

The results of the coupled PCA and TT analysis on the Fe K-edge EXAFS data indicate Fe-bearing chlorite and illite, goethite and pyrite as the most relevant model compounds to account for the Fe-bearing species in the studied sediments (Table S7; Fig. S18). Chlorite is here considered to account for Fe incorporated in the trioctahedral layer of the Fe-bearing clay minerals identified by TEM and XRD (*i.e.* greenalite/berthierine, chrysotile, and minor amounts of talc and chlorite; Fig. 4), whereas illite is considered to account for Fe incorporated in the dioctahedral layer of the Fe-bearing clay minerals identified by TEM and XRD (*i.e.* mostly smectite; Fig. 4). In addition, SEM-EDXS and TEM analyses support the selection of goethite as a relevant LC-LSF component (Fig S19), whereas SEM-EDXS and XRD analyses support the selection of pyrite (Figs. 3 and S12). The results of the LC-LSF fits of the Fe K-edge EXAFS spectra from the 21 studied sediments using these four components indicate that Fe-bearing clay minerals represent the largest contribution to Fe speciation (*i.e.* 65 - 85% of total Fe speciation), with a dominant contribution from Fe-bearing dioctahedral clay minerals (*i.e.* 40 - 60 % of total Fe speciation). The contribution of goethite ranges from 10 to 35% of total Fe speciation, whereas that of pyrite remains below 15% of total Fe speciation (Figs. 5 and S18; Table S8). Pyrite appears to significantly contribute to Fe speciation only in the sediments close to the shoreline in the three bays (*i.e.* KTV, VE2 and ST16), whereas it is no more detectable at the Fe K-edge at the other stations (Figs. 5 and S18). In the Vavouto Bay, the disappearance of pyrite from the shoreline to the reef appears to be compensated by an increase in the proportion of goethite, whereas it appears to be compensated by an increase of the proportion of Fe-rich trioctahedral clay minerals in the Kataviti Bay (Figs. 5 and S18; Table S8). In the Chasseloup Bay (ST16), the pyrite and Fe-rich trioctahedral clay minerals contributions are the highest among all the studied sediments, whereas the goethite contribution is the lowest. According to the results of the LC-LSF fits performed on the first-derivative of their Fe K-edge XANES spectra with the XANES spectra

of synthetic Fe(II) and Fe(III) talc model compounds, illite and chlorite are respectively considered to represent a Fe(III) and a Fe(II) pool (Fig. S20; Table S9). As a consequence, the results of the LC-LSF fits performed on the Fe K-edge EXAFS spectra from the studied sediments could be interpreted in terms of Fe(III)/Fe(II) ratio by attributing the proportions of illite and goethite to Fe(III) and those of chlorite and pyrite to Fe(II) (Figs. 5 and S18; Table S8). The results of this approach indicate that Fe mainly occurs as Fe(III) (*i.e.* 53 - 84% of total Fe) in all studied sediments. The highest Fe(II) fraction (*i.e.* 39% of total Fe) is found in the sediments in the Chasseloup Bay (ST16), whereas the lowest (*i.e.* 16% of total Fe) is found in the sediments the closer to the reef in the Vavouto Bay (LG2B). In addition, the fraction of Fe(II) decreases from the shore to the reef in the Vavouto Bay, whereas it remains constant in the Kataviti Bay (Figs. 5 and S18; Table S8). Given the uncertainties reported in Table S8, similar results were obtained by direct LC-LS fitting of the first-derivative of the Fe K-edge XANES data from the sediment samples with the Fe(II) and Fe(III) synthetic talc model compounds.

The results of the coupled PCA and TT analysis on the Ni K-edge EXAFS data indicate Ni-rich serpentine, Ni-dilute montmorillonite and goethite as the most relevant model compounds (Table S10; Fig S21 and 22) to account for the Ni-bearing species in the studied sediment samples (Table S11; Fig S23). The Ni-rich serpentine model compound is here interpreted as a proxy for Ni incorporated in the trioctahedral layer of the 1/1 Fe-rich clay minerals (*i.e.* chrysotile and greenalite/berthierine) identified by TEM and XRD, and of talc and chlorite also identified in small amounts by XRD (Fig. S11). Indeed, the EXAFS signals from Ni and Fe second neighbors around Ni in the clay minerals layer are expected to be undistinguishable one from the other due to the close Z numbers of these two elements. The Ni-dilute montmorillonite model compound is interpreted as a proxy for Ni incorporated in the dioctahedral layer of the swelling smectites identified by TEM and XRD as a major clay

548 mineral in our samples. The results of the LC-LSF fits of the Ni K-edge EXAFS spectra from
549 the 21 studied sediments using these three components indicate that Ni speciation is largely
550 dominated by Fe-rich trioctahedral clay minerals (*i.e.* 36-63% of total Ni speciation), with a
551 lower contribution from Ni dioctahedral clay minerals (*i.e.* 13-46% of total Ni speciation) and
552 goethite (*i.e.* 12-35% of total Ni speciation) (Figs. 5 and S23; Table S11). For all studied
553 sediments, Ni speciation does not change significantly with depth (Fig. S23). In both the
554 Kataviti and Vavouto Bays, the contribution of Ni-rich trioctahedral clay minerals to Ni
555 speciation is found to remain stable (*i.e.* ~57% and 49%, respectively) from the shore to the
556 reef. In contrast, the contribution of goethite to Ni speciation increases, whereas that of Ni
557 dioctahedral clay minerals decreases (Figs. 5 and S23; Table S11). This latter trend is more
558 marked in the Vavouto Bay than in the Kataviti Bay. In the Chasseloup Bay, the contribution
559 of Ni dioctahedral clay minerals is larger than in the two other bays (Figs. 5 and S23; Table
560 S11).
561
562 **4. DISCUSSION**
563
564 **4.1. A major contribution of clay minerals to Fe and Ni speciation, compared to Fe-**
565 **oxides and Fe-sulfides**
566
567 The presence of Fe- and Ni-bearing clay minerals in the lagoon sediments downstream
568 lateritic outcrops in New Caledonia has already been reported by Fernandez et al. (2017) for
569 the Dumbéa Bay, which is located in the South-Western part of the main Island (Grande-
570 Terre). The results of our study in the North-Western part of the main Island show that these
571 Fe- and Ni-bearing clay minerals are in fact Fe-rich chrysotile, greenalite/berthierine, as well
572 as Fe-rich smectites (nontronite) and micas (glauconite). Our results also indicate that these

clay minerals are the major host for Fe and Ni in the lagoon sediments downstream of lateritic outcrops in New Caledonia. In addition to clay minerals, Fe-(oxyhydr)oxides have also been reported as possible hosts for Ni in the sediments from the Dumbéa Bay, but the method employed (*i.e.* sequential chemical extractions) precluded a precise identification of these Fe-(oxyhydr)oxides (Ambatsian et al., 1997). Thanks to its direct evaluation of Ni and Fe speciation (*i.e.* synchrotron-based XAS data), our study shows that goethite is the Ni-bearing Fe-(oxyhydr)oxides in the lagoon sediments from New Caledonia. In addition, it also indicates that this mineral phase can account for up to 35% of total Ni speciation, this upper value being observed close to the coral reef in the Vavouto Bay. Finally, our results show that the redox state of Fe in the studied lagoon sediments, that were carefully preserved from oxidation during sampling, storage and analysis, is dominated by Fe(III) (*i.e.* 60 – 80% of total Fe). Despite the significant amounts of Fe(II) that can be found in the studied sediments (*i.e.* 20 – 40% of total Fe), pyrite appears as a scarce host for Fe and it does not contribute to Ni speciation at a detectable level in any of the studied samples. However, because of the known possible substitution of Ni^{2+} ions for Fe^{2+} ions within the structure of Fe-sulfides, a small contribution of these mineral phases to Ni speciation cannot be dismissed. In the same way, the carbonate minerals (*i.e.* calcite, magnesian calcite and aragonite) that can represent up to 70% of the mineral fraction in the sediments of the Vavouto Bay (Fig. 3; Table S3) do not appear to contribute at a detectable level to Fe and Ni speciation in any of the studied sediments. However, because of the known possible substitution of Fe^{2+} and Ni^{2+} ions for Ca^{2+} ions within the structure of calcite (Dromgoole and Walter, 1990, Hoffman and Stipp, 2001, Lakshtanov and Stipp, 2007; Mettler et al. 2009) and aragonite (Mejri et al., 2015), a small contribution of these mineral phases to both Ni and Fe speciation cannot be dismissed.

All the above-mentioned results indicate that in the studied lagoon sediments Fe is hosted by 2/1 clay minerals (mainly smectite and glauconite) for about one half, and by 1/1 clay

598 minerals (mainly chrysotile and greenalite/berthierine), goethite and minor amounts of pyrite
599 for the other half, whereas Ni is hosted by 1/1 clay minerals for about one half, and by 2/1
600 clay minerals and goethite for the other half. Along with detailed mineralogy and sediments
601 chemistry, the evolution of these Fe and Ni speciation along a shore-to-reef gradient helps to
602 draw a general sketch of the influence of the redox state of the sediments on Fe and Ni
603 crystal-chemistry and to assess the actual origin of pyrite and Fe/Ni clay minerals in the
604 lagoon sediments of New Caledonia.
605
606 **4.2 A contrasted origin for the various Fe- and Ni-bearing mineral phases in the studied**
607 **lagoon sediments**
608
609 Among the three types of Ni-bearing clay minerals identified in the studied lagoon sediments,
610 the first one is a Fe-rich 1/1 trioctahedral phyllosilicate identified as chrysotile. This type of
611 clay minerals has already been recognized as one of the Ni-bearing mineral phases in the
612 Koniambo ultramafic outcrop (Dublet et al., 2012; Fritsch et al., 2016; 2019), as well as in the
613 mangrove sediments of the Vavouto Bay (Noël et al., 2014; 2015) located upstream of the
614 studied lagoon sediments. Therefore, the Ni-bearing chrysotile observed in the studied lagoon
615 sediments is most likely inherited from erosion of the Koniambo lateritic outcrops. The
616 second type of Ni-bearing clay mineral recognized in the studied sediments are Fe-rich 1/1
617 trioctahedral clay minerals identified as greenalite/berthierine. TEM-EDXS analyses show
618 that these Fe-rich 1/1 trioctahedral clay minerals correspond to the most Ni-rich mineral
619 phases observed in the studied sediments (Table 2). The significantly higher Fe content of
620 these clay minerals (between 41 and 54 wt% FeO; Table 2) compared to that in the clay
621 minerals from the saprolite and laterite units of the Koniambo outcrop (at most 7.5wt % FeO;
622 Fritsch et al., 2019) supports the authigenic origin of greenalite/berthierine in the lagoon

623 sediments. This hypothesis is also supported by the authigenic origin reported by Bailey
624 (1988) for odinite, a Fe-rich green clay that is found in shallow marine shelf and reef lagoon
625 at tropical latitudes (Ku and Walter, 2003; Morard et al., 2010). It is noteworthy that odinite
626 can not be confused with the greenalite/berthierine Fe-rich clays identified by TEM-EDXS in
627 our study since it is significantly richer in Mg (Fig. 4; Table 2). Finally, the third type of Ni-
628 bearing clay minerals recognized in the studied lagoon sediments is a Fe-rich 2/1 dioctahedral
629 phyllosilicate identified as both glauconite and smectite (Fig. 4; Table 2). Although the
630 authigenic origin of glauconite is widely accepted, the origin of smectite has to be discussed
631 in the present context. This clay mineral has been scarcely detected in the Koniambo outcrop,
632 but the Vertisols and Cambisols that developed on the surrounding volcano-sedimentary
633 settings (Fritsch, 2012) can contain significant amounts of smectite. In addition, the Fe-rich
634 2/1 dioctahedral clay mineral identified as smectite in the studied lagoon sediments shows
635 strong similarities with the Fe-rich nontronite already reported as a major Fe and Ni host in
636 the mangrove sediments of the Vavouto Bay (Noël et al., 2014; 2015). Therefore, the Fe-rich
637 smectite found as one of the Ni-bearing clay minerals in the studied lagoon sediments can be
638 considered as inherited from upstream mangrove sediments and/or Vertisols and Cambisols.
639 Altogether, these results indicate that Fe dominantly occurs as Fe(III) in the studied lagoon
640 sediments, and that the major fraction of this Fe(III) is hosted by Fe-rich 2/1 dioctahedral clay
641 minerals that are either inherited (*i.e.* smectite/nontronite) or authigenic (*i.e.* glauconite). In
642 contrast, Ni is mainly hosted by authigenic Fe(II)-bearing 1/1 trioctahedral clay minerals (*i.e.*
643 greenalite/berthierine).
644 In addition to clay minerals, the two Fe-sulfides (*i.e.* mackinawite and pyrite) that have been
645 recognized as a host for Fe(II) in the studied sediments (Fig. 5) are considered as mainly
646 authigenic. This assumption relies on the fact that pyritization is a well-known process for
647 marine sediments (Huerta-Diaz et al., 1992; Lovley and Chapelle, 1995; Wang and Morse,

1996, Morse and Wang 1997, Neretin et al. 2004, Li et al., 2007; Wang et al., 2012). It is in agreement with S speciation, which shows a global increase of both the fraction of S as sulfides and the pyrite/mackinawite ratio with depth (Fig. S15; Table S6). It is also in agreement with Fe speciation, which shows an increase of Fe(II) with depth in the sediments close to the shore for the Kataviti and Vavouto Bays (*i.e*. KTV and VE2; Fig. S18). These trends strongly supports the hypothesis of an *in-situ* pyritization through the formation of intermediate mackinawite that further transforms to pyrite upon ageing during early diagenesis, as proposed by several authors (Morse at al., 1987; Rickard and Luther, 1997; 2007; Wilkin and Barnes, 1997; Benning et al., 2000). However, a possible contribution from the nearby mangrove sediments to the pyrite found in the sediments close to the shore cannot be dismissed. Firstly, because previous studies performed on mangrove sediments located upstream of the Vavouto Bay demonstrated the occurrence of large amounts of pyrite at depth (Noël et al., 2014; 2015). Secondly, because the correlation plot between the fraction of S as sulfides and the TOC depicted in Figure S24 suggests that the fraction of S as sulfides in the sediments at the VE2 station (*i.e*. the closest to the mangrove in the Vavouto Bay) is larger than that expected following the linear regression line.

Finally, goethite (*i.e*. the only Fe(III)-oxide identified in the studied lagoon sediments and which also contributes to Ni hosting) is considered as mainly inherited from the Koniambo because of its large occurrence in this lateritic outcrop (Fandeur et al., 2009a; 2009b; Dublet et al., 2102; 2014). In addition, a minor inheritance from mangrove sediments can not be ruled out since a precedent study suggested a possible role of the tidal cycle on the partial oxidation of pyrite and subsequent goethite formation in mangrove sediments (Noël et al., 2017). However, a partial authigenic origin for goethite might also be supported by the increasing contribution of this Fe-oxide to Fe speciation across the shore-to-reef gradient in the Vavouto Bay (see discussion below).

673

674 **4.3. Influence of the redox conditions on Fe and Ni speciation in the studied sediments**

675

676 The results of dissolved oxygen micro-profiling performed at the sediment/water interface
677 indicate anoxic conditions below a maximum depth of 5 mm in all the studied sediments (Fig.
678 S1). However, Fe K-edge XAS results indicate major occurrence of Fe(III) in the studied
679 sediments (Figs. 5 and S18). This apparent discrepancy could be related to a limited anaerobic
680 Fe reduction compared to the global Fe(III) pool. For instance, Fe(III) in crystalline oxides
681 (*i.e.* goethite) would be better preserved from bacterial reduction than Fe(III) in amorphous
682 oxides (*i.e.* ferrihydrite) even in organic rich sediments (Taylor and MacQuaker, 2011; Barber
683 et al., 2017). In addition, the TOC measured in the studied lagoon sediments *(i.e.* 1.0-4.5
684 wt%; Table S1; Figs. S2; S3 and S4) is significantly lower than that measured in the nearby
685 mangrove sediments (*i.e.* 5-15% beneath *Rhizophora* stand; Marchand et al., 2012; Noël et
686 al., 2015) where Fe reduction was found to be complete with euxinic conditions leading to
687 intense pyritisation (Noël et al., 2015). These results suggest a possible limitation of the TOC
688 pool compared to the Fe(III) pool to explain the low amounts of Fe(II) measured in the
689 studied lagoon sediments. This hypothesis is supported by the higher Fe(II) fraction and TOC
690 content in the Chasseloup Bay (*i.e.* 40% of total Fe and around 4.5 wt%, respectively)
691 compared to the two other bays (*i.e.* Fe(II) fraction between 20 to 30% of total Fe and TOC
692 between 1.0 and 3.5 wt%). It is also supported by the similar decreasing trend that can be
693 observed for TOC and Fe(II) as a function of the distance to the shore in the Vavouto Bay (*i.e.*
694 TOC from 2.5 to 1.0 wt% and Fe(II) from 35 to 15% of total Fe; Figs. 5 and S18; Table S8).
695 Although, this trend is not observed in the Kataviti Bay where the Fe(II) fraction remains
696 constant around 20% of total Fe along the shore-to-reef gradient despite a decreasing TOC
697 (*i.e.* from 3.5 to 2.0 wt%; Figs. 5 and S18; Table S8), the amount of Fe(II) in the studied

698 lagoon sediments appears to be roughly correlated to the TOC content (Fig. S24). Despite
699 relatively high Fe concentrations compared to other lagoon settings (*i.e.* 0.17-4.58 wt% Fe;
700 Morisson et al., 2010; Magallanes-Ordóñez et al., 2015) and coastal sediments (*i.e.* 0.2-7 wt%
701 Fe; Anbuselvan et al., 2018; Koukina et al., 2017) under tropical climate, this correlation
702 suggests that TOC might be a limiting factor for Fe(III) microbial reduction (and in turn,
703 pyritization) in the studied Fe-rich lagoon sediments of New Caledonia. This limiting
704 character of the TOC available to fuel microbial reduction of Fe(III) associated with goethite
705 and/or clay minerals has already been proposed to explain the low formation of pyrite in
706 subsurface redox transition zone or sediments (Benzine et al., 2013; Sabadini-Santos et al.,
707 2014; Wu et al., 2017).
708 In addition to the limiting character of TOC compared to the large Fe(III) pool, sediments re-
709 suspension could also contribute to the limited microbial reduction of Fe(III) in the studied
710 sediments (Bataillard et al., 2014). This hypothesis is supported by the shallow character of
711 the studied lagoon (*i.e.* not more than 40 m, with a large portion less than 20 m deep;
712 Wattelez et al., 2016) and the high frequency of windy and cyclonic events reported in the
713 South-East Pacific region (Lavigne et Sahal, 2011, Forsberg et al., 2012). A recent study in
714 the similar South-West lagoon of New Caledonia demonstrated the influence of these
715 parameters on the dispersion and transport of suspended particulate matter (Fernandez et al.,
716 2017). Following this hypothesis, the Vavouto Bay is expected to be more exposed to
717 sediments re-suspension because of stronger currents in relation with the proximity of a reef
718 pass (Fig. 1). This latter hypothesis is supported by the significant increase in the fraction of
719 Fe(III) across the shore-to-reef gradient in this bay, which is related to the net increase in the
720 fraction of Fe(III) in goethite and the concomitant decrease of Fe(II) in pyrite when
721 approaching the coral reef (Figs. S5 and S18; Table S8). In comparison, the fraction of Fe(III)
722 in the Kataviti Bay does not change significantly across the shore-to-reef gradient because the

723 decrease of Fe(II) in pyrite is compensated by an increase of Fe(II) in clay minerals (*i.e.*
724 chrysotile and/or greenalite/berthierine; Figs. S5 and S18; Table S8). It is noteworthy that
725 pyrite is detected by EXAFS at the Fe K-edge only in the sediments the closest to the shore
726 and that this fraction remains below 14% of total Fe in all studied sediments (Figs. 5 and S18;
727 Table S8). However, the proposed difference in the redox conditions as a function of the
728 distance to the shore between the Vavouto and the Kataviti Bays is also supported by S
729 speciation. Indeed, S K-edge XANES data indicate a larger decrease of the proportion of S as
730 sulfides from the shore to the reef in the Vavouto Bay (*i.e.* mean value from 94% to 36% of
731 total S; Table S6) compared to the Kataviti Bay (*i.e.* mean value from 82% to 45% of total S;
732 Table S6).
733 Altogether, these observations suggest that the top layers of the studied lagoon sediments are
734 more or less regularly exposed to oxidation events due to partial re-suspension that are not
735 favorable to the development of sulfidic conditions. Such oscillating redox conditions likely
736 explains the importance of clay minerals on Fe and Ni speciation compared to pyrite because
737 of the better stability of Fe(II)-phyllosilicates in oxic-suboxic conditions compared to Fe(II)-
738 sulfides (Luther, 1987; Morse et al., 1987; Luther et al., 1992; Wilson et al., 2006; Dong et
739 al., 2009; Dzene et al., 2018; Rickard and Luther, 2007). In addition, this more or less regular
740 re-oxidation of the top layers of the studied sediments could have important implications on
741 the potential remobilization of the trace metals that are associated with pyrite (Huerta-Diaz et
742 al., 1992, 1998, Scholz and Neumann, 2007, Neumann et al., 2013, Noël et al., 2015, Le Pape
743 et al., 2016), especially Ni-rich pyrite that could be inherited from the mangrove sediments
744 (Noël et al., 2015). Interestingly, the pyrite grains that we observed in the lagoon sediment
745 were found to be either devoid of Ni or to host very low amounts of Ni. These observations
746 are in agreement with the findings of Noël et al. (2015) that the smallest pyrite grains, which
747 are the richest in Ni, are also the most sensitive to oxidation, especially in the sediments

beneath the *Rhizophora* stand that are the most exposed to re-aeration (0-50 cm depth) due to tidal pumping on banks along mangrove channels and bio-irrigation by benthic macrofauna in inner *Rhizophora* mangrove. If one expects a partial contribution of the mangrove sediments to the pool of pyrite in the lagoon sediments, only the largest pyrite grains that are the poorest in Ni should be concerned because they show the largest stability (*i.e*. lowest solubilization rates). Further studies on the relative reactivity of pyrite and Fe(II)-bearing clay minerals during simulated redox cycling would help to better evaluate the contribution of this mechanism to the dynamics of trace metals in the lagoon sediments of New Caledonia, and more largely in tropical lagoon sedimentary settings.

5. CONCLUSION

The results of this study indicate that goethite (*i.e*. the most abundant mineral phase in the upstream lateritic outcrop) account at most for 30% of total Ni speciation in the studied lagoon sediments. Despite the significant amounts of Fe(II) (*i.e*. up to 40% of total Fe) that can be found in some of the studied sediments, pyrite appears as a scarce host for Fe that is detected only at the stations close to the shore. More importantly, it does not contribute to Ni speciation at a detectable level in the studied lagoon sediments. On the opposite, Fe(II)-rich 1/1 trioctahedral clay minerals identified as chrysotile and greenalite/berthierine, as well as Fe(III)-rich 2/1 dioctahedral clay minerals identified as nontronite and glauconite appear as the major hosts for Fe and Ni in lagoon sediments downstream of lateritic outcrops in New Caledonia. Chrysotile is considered as inherited from either the lateritic outcrop and/or the nearby mangrove sediments, whereas greenalite/berthierine is considered as authigenic. Glauconite is also considered as authigenic, whereas the source of smectite is more controversial since it could originate from the nearby mangrove sediments or soils developed

upon volcano-sedimentary settings (*i.e*. Vertisols and/or Cambisols) or have formed *in situ* upon early diagenesis. The better stability of Fe(II)-bearing clay minerals in oxic-suboxic conditions compared to Fe(II)-sulfides could explain their importance in these shallow Fe-rich sedimentary settings that are subjected to more or less regular re-oxidation events due to re-suspension of the sediments top-layers. In tropical lagoon environments, green clays authigenesis might thus represent a key process in the scavenging of trace metals, especially Fe and Ni (and possibly Cr), that are delivered to the shoreline ecosystems by continental erosion. From a geological perspective, this latter point suggests that the underestimated importance of green clays authigenesis recently proposed for the geological cycling of Fe (Rasmussen et al., 2014a; 2014b; 2015; 2016; 2017; Balderman et al., 2015; 2017; Konhauser et al., 2017) might not only concern deep-sea sediments, but also Fe-rich shallow lagoon sedimentary settings. In addition, regarding the hosting capacity of greenalite/berthierine towards Ni (and possibly Cr) demonstrated in our study, green clays authigenesis might also play, or have played, an important role on the coastal geological cycles of a large set of trace metals. From an environmental perspective, the results of this study suggest that the reactivity of clay minerals, and especially green clays, towards trace metals upon early diagenesis should be more largely considered in ecotoxicological study aimed at evaluating the potential threat of continental inputs towards the benthic biodiversity in tropical lagoon sedimentary settings.

ACKNOWLEDGEMENTS

We thank Imène Estève, Béeatrice Doisneau and Stéphanie Delbrel for their help in SEM analyses as well as Ludovic Delbes for his help in XRD analyses. We also acknowledge Isabelle Kieffer and Gautier Landrot for their help on the FAME-CRG beamline at ESRF and

on the SAMBA beamline at SOLEIL respectively as well as Matthew Latimer and Eric Nelson, as well as Ryan Davis for their help during measurements at the 9-3 and 4-1 SSRL beamline respectively. A part of this study was funded by the CNRT (Centre National de Recherche Technologique sur le nickel et son environnement - www.cnrt.nc) through the DYNAMINE project (2015-2018).

CONFLICT OF INTEREST

The authors declare that they have no conflict of interest.

REFERENCES

Álvarez-Iglesias, P., Rubio, B., 2012. Early diagenesis of organic-matter-rich sediments in a ría environment: Organic matter sources, pyrites morphology and limitation of pyritization at depth. Estuarine, Coastal and Shelf Science 100, 113–123. https://doi.org/10.1016/j.ecss.2012.01.005

Ambatsian, P., Fernex, F., Bernat, M., Parron, C., Lecolle, J., 1997. High metal inputs to closed seas: the New Caledonian lagoon. Journal of Geochemical Exploration 59, 59–74. https://doi.org/10.1016/S0375-6742(96)00020-9

Anbuselvan, N., Senthil Nathan, D., Sridharan, M., 2018. Heavy metal assessment in surface sediments off Coromandel Coast of India: Implication on marine pollution. Marine Pollution Bulletin 131, 712–726. https://doi.org/10.1016/j.marpolbul.2018.04.074

Andréfouët, S., Cabioch, G., Flamand, B., Pelletier, B., 2009. A reappraisal of the diversity of geomorphological and genetic processes of New Caledonian coral reefs: a synthesis from

822 optical remote sensing, coring and acoustic multibeam observations. Coral Reefs, 28, 691–
823 707. https://doi.org/10.1007/s00338-009-0503-y

824 Andréfouët, S., Wantiez, L., 2010. Characterizing the diversity of coral reef habitats and fish
825 communities found in UNESCO World Heritage Areas: the strategy applied for New-
826 Caledonia. Marine Pollution Bulletin, 61, 612–620. https://doi.org/10.1016/j.marpolbul.
827 2010.06.031

828 Bailey, S.W., 1988. Odinite, a new dioctahedral-trioctahedral Fe3+-rich 1:1 clay mineral.
829 Clay Minerals 23, 237–247. https://doi.org/10.1180/claymin.1988.023.3.01

830 Baldermann, A., Dietzel, M., Mavromatis, V., Mittermayr, F., Warr, L.N., Wemmer, K.,
831 2017. The role of Fe on the formation and diagenesis of interstratified glauconite-
832 smectite and illite-smectite: A case study of Upper Cretaceous shallow-water
833 carbonates. Chemical Geology 453, 21–34.
834 https://doi.org/10.1016/j.chemgeo.2017.02.008

835 Baldermann, A., Warr, L.N., Letofsky-Papst, I., Mavromatis, V., 2015. Substantial iron
836 sequestration during green-clay authigenesis in modern deep-sea sediments. Nature
837 Geoscience 8, 885–889. https://doi.org/10.1038/ngeo2542

838 Barber, A., Brandes, J., Leri, A., Lalonde, K., Balind, K., Wirick, S., Wang, J., Gélinas, Y.,
839 2017. Preservation of organic matter in marine sediments by inner-sphere interactions
840 with reactive iron. Scientific Reports 7, 366. https://doi.org/10.1038/s41598-017-
841 00494-0

842 Bataillard, P., Grangeon, S., Quinn, P., Mosselmans, F., Lahfid, A., Wille, G., Joulian, C.,
843 Battaglia-Brunet, F., 2014. Iron and arsenic speciation in marine sediments
844 undergoing a resuspension event: the impact of biotic activity. Journal of Soils and
845 Sediments 14, 615–629. https://doi.org/10.1007/s11368-013-0829-5

Beauvais, A., Parisot, J.-C., Savin, C., 2007. Ultramafic rock weathering and slope erosion processes in a South West Pacific tropical environment. Geomorphology 83, 1–13. https://doi.org/10.1016/j.geomorph.2006.06.016

Benning, L., Wilkin, R.T., Barnes, H.L., 2000. reaction pathway in the Fe-S- system below 100°C. Chemical Geology, 167, 25. https://doi.org/10.1016/S0009-2541(99)00198-9

Benzine, J., Shelobolina, E., Xiong, M.Y., Kennedy, D.W., McKinley, J.P., Lin, X., Roden, E.E., 2013. Fe-phyllosilicate redox cycling organisms from a redox transition zone in Hanford 300 Area sediments. Frontiers in Microbiology 4. https://doi.org/10.3389/fmicb.2013.00388

Berar, J.F., 1990. Reduction of the number of parameters in real time Rietveld refinement. I. U. Cr. Sat. Meeting Powder diffraction, Toulouse, 1990.

Berner, Z.A., Puchelt, H., NöLtner, T., Kramar, U., 2013. Pyrite geochemistry in the Toarcian Posidonia Shale of south-west Germany: Evidence for contrasting trace-element patterns of diagenetic and syngenetic pyrites: *Pyrite element geochemistry*. Sedimentology 60, 548–573. https://doi.org/10.1111/j.1365-3091.2012.01350.x

Birch, G.F., 2017. Determination of sediment metal background concentrations and enrichment in marine environments – A critical review. Science of The Total Environment 580, 813–831. https://doi.org/10.1016/j.scitotenv.2016.12.028

Bonnin D., Calas G., Suquet H. and Pezerat H. (1985) Sites occupancy of Fe3+ in Garfield nontronite: a spectroscopic study. Phys. Chem. Miner. 12, 55-64. https://doi.org/10.1007/BF00348748

Botsou, F., Godelitsas, A., Kaberi, H., Mertzimekis, T.J., Goettlicher, J., Steininger, R., Scoullos, M., 2015. Distribution and partitioning of major and trace elements in pyrite-bearing sediments of a Mediterranean coastal lagoon. Geochemistry 75, 219–

236. https://doi.org/10.1016/j.chemer.2015.02.001

Brindley G. and Brown G. (1980) Crystal structures of clay minerals and their X-ray identification. Mineral. Soc. Monogr. 5, 495p.

Burton, E.D.., Sullivan, L.A, Bush, R.T, and Powell, B. 2008. Iron-sulfide and trace element behaviour in sediments of Coombabah Lake, southern Moreton Bay (Australia). Marine Pollution Bulletin 564, 1353–1376. https://doi.org/10.1016/j.marpolbul.2008.04.012

Butler, I.B., Rickard, D., 2000. Framboidal pyrite formation via the oxidation of iron (II) monosulfide by hydrogen sulphide. Geochimica et Cosmochimica Acta 64, 2665–2672. https://doi.org/10.1016/S0016-7037(00)00387-2

Cabioch, G., Courrege, T., Turpin, L., Castellaro, C. Recy, J. 1999. Development patterns of fringing and barrier reefs in New Caledonia (southwest Pacific). Oceanologica Acta, 22, 567-578. https://doi.org/10.1016/S0037-0738(03)00094-0

Cabioch, G. 2003. Postglacial reef development in the South-West Pacific : case studies from New Caledonia and Vanuatu. Sedimentary Geology, 159, 43-59. https://doi.org/10.1016/S0037-0738(03)00094-0

Coates-Marnane, J., Olley, J., Burton, J., Grinham, A., 2016. The impact of a high magnitude flood on metal pollution in a shallow subtropical estuarine embayment. Science of The Total Environment 569-570, 716–731. https://doi.org/10.1016/j.scitotenv.2016.06.193

Cornell, R., Schwertmann, U., 2003. The Iron Oxides: Structure, Properties, Reactions, Occurrences, And Uses.

~~Cornu, S., Clozel B., Extractions séquentielles et spéciation des éléments trace métalliques dans les sols naturels. Analyse critique, 7, 179-189.~~

893 Cuong, D.T., Obbard, J.P., 2006. Metal speciation in coastal marine sediments from
894 Singapore using a modified BCR-sequential extraction procedure. Applied
895 Geochemistry 21, 1335–1346. https://doi.org/10.1016/j.apgeochem.2006.05.001

896 Dalto, A.G., Grémare, A., Dinet, A., Fichet, D., 2006. Muddy-bottom meiofauna responses to
897 metal concentrations and organic enrichment in New Caledonia South-West Lagoon.
898 Estuarine, Coastal and Shelf Science 67, 629–644.
899 https://doi.org/10.1016/j.ecss.2006.01.002

900 Debenay, J.P., Fernandez, J.M., 2009. Benthic foraminifera records of complex anthropogenic
901 environmental changes combined with geochemical data in a tropical bay of New
902 Caledonia (SW Pacific). Marine Pollution Bulletin, 59 (8–12), 311–322.
903 https://doi.org/10.1016/j.marpolbul.2009.09.014

904 Díaz-de-Alba, M., Huerta-Diaz, M.A., Delgadillo-Hinojosa, F., Hare, L., Galindo-Riaño,
905 M.D., Siqueiros-Valencia, A., 2016. Trace metals partitioning among different
906 sedimentary mineral phases and the deposit-feeding polychaete Armandia brevis.
907 Science of The Total Environment 543, 248–266.
908 https://doi.org/10.1016/j.scitotenv.2015.11.033

909 Di Toro, D.M., Mahony, J.D., Hansen, D.J., Scott, K.J., Carlson, A.R., Ankley, G.T., 1992.
910 Acid volatile sulfide predicts the acute toxicity of cadmium and nickel in sediments.
911 Environmental Science & Technology 26, 96–101.
912 https://doi.org/10.1021/es00025a009

913 Dong, H., Jaisi, D.P., Kim, J., Zhang, G., 2009. Microbe-clay mineral interactions. American
914 Mineralogist 94, 1505–1519. https://doi.org/10.2138/am.2009.3246

915 Dromgoole, E.L., Walter, L.M., 1990. Iron and manganese incorporation into calcite: Effects
916 of growth kinetics, temperature and solution chemistry. Chemical Geology 81, 311–

336. https://doi.org/10.1016/0009-2541(90)90053-A

Dublet, G., Juillot, F., Brest, J., Noël, V., Fritsch, E., Proux, O., Olivi, L., Ploquin, F., Morin, G., 2017. Vertical changes of the Co and Mn speciation along a lateritic regolith developed on peridotites (New Caledonia). Geochimica et Cosmochimica Acta 217, 1–15. https://doi.org/10.1016/j.gca.2017.07.010

Dublet, G., Juillot, F., Morin, G., Fritsch, E., Noël, V., Brest, J., Brown, G.E., 2014. XAS evidence for Ni sequestration by siderite in a lateritic Ni-deposit from New Caledonia. American Mineralogist 99, 225–234. https://doi.org/10.2138/am.2014.4625

Dublet, G., Juillot, F., Morin, G., Fritsch, E., Fandeur, D., Ona-Nguema, G., Brown, G.E., 2012. Ni speciation in a New Caledonian lateritic regolith: A quantitative X-ray absorption spectroscopy investigation. Geochimica et Cosmochimica Acta 95, 119–133. https://doi.org/10.1016/j.gca.2012.07.030

Dupouy, C., Neveux, J., Ouillon, S., Frouin, R., Murakami, H., Hochard, S., Dirberg, G. 2010. Inherent optical properties and satellite retrieval of chrorophyll concentration in the lagoon and open ocean waters of New Caledonia. Marine Pollution Bulletin, 61, 503-518. https://doi.org/10.1016/j.marpolbul.2010.06.039

Dzene, L., Brendlé, J., Limousy, L., Dutournié, P., Martin, C., Michau, N., 2018. Synthesis of iron-rich tri-octahedral clay minerals: A review. Applied Clay Science 166, 276–287. https://doi.org/10.1016/j.clay.2018.09.030

Elias, M., Donaldson, M.J., Giorgetta, N.E., 1981. Geology, mineralogy, and chemistry of lateritic nickel-cobalt deposits near Kalgoorlie, Western Australia. Economic Geology 76, 1775–1783. https://doi.org/10.2113/gsecongeo.76.6.1775

Fandeur, D., Juillot, F., Morin, G., Olivi, L., Cognigni, A., Ambrosi, J.-P., Guyot, F., Fritsch, E., 2009. Synchrotron-based speciation of chromium in an Oxisol from New

941 Caledonia: Importance of secondary Fe-(oxyhydr)oxides. American Mineralogist 94,
942 710–719. https://doi.org/10.2138/am.2009.3073

943 Fandeur, D., Juillot, F., Morin, G., Olivi, L., Cognigni, A., Webb, S.M., Ambrosi, J.-P.,
944 Fritsch, E., Guyot, F., Brown, Jr., G.E., 2009. XANES Evidence for Oxidation of
945 Cr(III) to Cr(VI) by Mn-Oxides in a Lateritic Regolith Developed on Serpentinized
946 Ultramafic Rocks of New Caledonia. Environmental Science & Technology 43, 7384–
947 7390. https://doi.org/10.1021/es900498r

948 Fernandez, J.-M., Meunier, J.-D., Ouillon, S., Moreton, B., Douillet, P., Grauby, O., 2017.
949 Dynamics of Suspended Sediments during a Dry Season and Their Consequences on
950 Metal Transportation in a Coral Reef Lagoon Impacted by Mining Activities, New
951 Caledonia. Water 9, 338. https://doi.org/10.3390/w9050338

952 Fernandez, J.-M., Ouillon, S., Chevillon, C., Douillet, P., Fichez, R., Gendre, R.L., 2006. A
953 combined modelling and geochemical study of the fate of terrigenous inputs from
954 mixed natural and mining sources in a coral reef lagoon (New Caledonia). Marine
955 Pollution Bulletin 52, 320–331. https://doi.org/10.1016/j.marpolbul.2005.09.010

956 Fichez, R., Chifflet, S., Douillet, P., Gérard, P., Gutierrez, F., Jouon, A., Ouillon, S., Grenz,
957 C., 2010. Biogeochemical typology and temporal variability of lagoon waters in a coral
958 reef ecosystem subject to terrigeneous and anthropogenic inputs (New Caledonia). Marine
959 Pollution Bulletin, 61, 309–322. https://doi.org/10.1016/ /j.marpolbul.2010.06.021

960 Forsberg, P.L., Ernstsen, V.B., Andersen, T.J., Winter, C., Becker, M., Kroon, A., 2018. The
961 effect of successive storm events and seagrass coverage on sediment suspension in a
962 coastal lagoon. Estuarine, Coastal and Shelf Science 212, 329–340.
963 https://doi.org/10.1016/j.ecss.2018.07.006

~~Freyssinet, P., Butt, C.R.M., Morris, R., 2005. Ore-forming processes related to lateritic weathering.~~

Fritsch, E., Juillot, F., Dublet, G., Fonteneau, L., Fandeur, D., Martin, E., Caner, L., Auzende, A.-L., Grauby, O., Beaufort, D., 2016. An alternative model for the formation of hydrous Mg/Ni layer silicates ('deweylite'/'garnierite') in faulted peridotites of New Caledonia: I. Texture and mineralogy of a paragenetic succession of silicate infillings. European Journal of Mineralogy 28, 295–311. https://doi.org/10.1127/ejm/2015/0027-2503

Fritsch E (2012) Les sols. In: Atlas de la Nouvelle-Calédonie, Bonvallot J, Gay J-C, Habert E (eds). IRD & Congrès de la Nouvelle-Calédonie, Marseille

Fu, W., Zhang, Y., Pang, C., Zeng, X., Huang, X., Yang, M., Shao, Y., Lin, H., 2018. Garnierite mineralization from a serpentinite-derived lateritic regolith, Sulawesi Island, Indonesia: Mineralogy, geochemistry and link to hydrologic flow regime. Journal of Geochemical Exploration 188, 240–256. https://doi.org/10.1016/j.gexplo.2018.01.022

Gagnon, C., Mucci, A., Pelletier, É., 1995. Anomalous accumulation of acid-volatile sulphides (AVS) in a coastal marine sediment, Saguenay Fjord, Canada. Geochimica et Cosmochimica Acta 59, 2663–2675. https://doi.org/10.1016/0016-7037(95)00163-T

Georep (2019) Service de la Géomatique de la Direction des Technologies et des Services de l'information, https://georep.nc

Gleeson, S.A., Herrington, R.J., Durango, J., Velásquez, C.A., 2004. The Mineralogy and Geochemistry of the Cerro Matoso S.A. Ni Laterite Deposit, Montelíbano, Colombia. Economic Geology, 99, 1197-1213. http://doi.org/10.2113/99.6.1197

987 Golithtly J.P. and Arancibia O.N. (1979) The chemical composition and infrared spectrum of
988 nickel- and iron-substituteed serpentine from a nickeliferous laterite profile, Soroako,
989 Indonesia. Canadian Mineralogist, 17, 719-728.

990 Grenz , C., Le Borgne, R., Fichez, R. Torreton J.P. 2010a. Tropical lagoon multidisciplinary
991 investigations : An overview of the PNEC New Caledonia pilot site. Marine Pollution
992 Bulletin, 61, 267-268. https://doi.org/10.1016/j.marpolbul.2010.06.030

993 Grenz , C., Denis, L., Pringault, O., Fichez, R. 2010b. Spatial and seasonal variability of
994 sediment oxygen consumption and nutrient fluxes at the sediment water interface in a sub-
995 tropical lagoon (New Caledonia). Marine Pollution Bulletin, 61, 399–412.
996 https://doi.org/10.1016/j.marpolbul.2010.06.014

997 Hoffmann, U., Stipp, S.L.., 2001. The behavior of Ni 2+ on calcite surfaces. Geochimica et
998 Cosmochimica Acta 65, 4131–4139. https://doi.org/10.1016/S0016-7037(01)00691-3

999 Hohmann C., Morin G., Ona-nguema G., Guigner J. M., Brown G. E. and Kappler A. (2011)
1000 Molecular-level modes of As binding to Fe (III) (oxyhydr)oxides precipitated by the
1001 anaer- obic nitrate-reducing Fe(II)-oxidizing Acidovorax sp. strain BoFeN1. Geochim.
1002 Cosmochim. Acta 75(17), 4699–4712. https://doi.org/10.1016/j.gca.2011.02.044

1003 Houles, A., Vincent, B., David, M., Ducousso, M., Galiana, A., Juillot, F., Hannibal, L.,
1004 Carriconde, F., Fritsch, E., Jourand, P., 2018. Ectomycorrhizal Communities
1005 Associated with the Legume Acacia spirorbis Growing on Contrasted Edaphic
1006 Constraints in New Caledonia. Microbial Ecology 76, 964–975.
1007 https://doi.org/10.1007/s00248-018-1193-1

1008 Huerta-Diaz, M.A., Muñoz-Barbosa, A., Otero, X.L., Valdivieso-Ojeda, J., Amaro-Franco,
1009 E.C., 2014. High variability in geochemical partitioning of iron, manganese and
1010 harmful trace metals in sediments of the mining port of Santa Rosalia, Baja California

1011 Sur, Mexico. Journal of Geochemical Exploration 145, 51–63.
1012 https://doi.org/10.1016/j.gexplo.2014.05.014

1013 Huerta-Diaz, M.A., Tessier, A., Carignan, R., 1998. Geochemistry of trace metals associated
1014 with reduced sulfur in freshwater sediments. Applied Geochemistry 13, 213–233.
1015 https://doi.org/10.1016/S0883-2927(97)00060-7

1016 Huerta-Diaz, M.A., Morse, J.W., 1992. Pyritization of trace metals in anoxic marine
1017 sediments. Geochimica et Cosmochimica Acta 56, 2681–2702.
1018 https://doi.org/10.1016/0016-7037(92)90353-K

1019 Ikogou, M., Ona-Nguema, G., Juillot, F., Le Pape, P., Menguy, N., Richeux, N., Guigner, J.-
1020 M., Noël, V., Brest, J., Baptiste, B., Morin, G., 2017. Long-term sequestration of
1021 nickel in mackinawite formed by Desulfovibrio capillatus upon Fe(III)-citrate
1022 reduction in the presence of thiosulfate. Applied Geochemistry 80, 143–154.
1023 https://doi.org/10.1016/j.apgeochem.2017.02.019

1024 Ildefonse Ph., Caberet D., Saincavit Ph., Calas G., Flank A.-M. and Lagarde P. (1998) Al X-
1025 ray absorption near edge strusture in model compound and earth's surface minerals.
1026 Phys. Chem. Minerals 25, 112–121. https://doi.org/10.1007/s002690050093

1027

1028 Jacquet, S., Delesalle, B., Torréton, J.-P., Blanchot, J. 2006. Responses of the phytoplankton
1029 communities to increased anthropogenic influences (Southwestern Lagoon, New
1030 Caledonia). Marine Ecology Progress Series, 320, 65–78.
1031 https://doi.org/10.3354/meps320065

1032 Janot, N., Lezama Pacheco, J.S., Pham, D.Q., O'Brien, T.M., Hausladen, D., Noël, V.,
1033 Lallier, F., Maher, K., Fendorf, S., Williams, K.H., Long, P.E., Bargar, J.R., 2016.
1034 Physico-Chemical Heterogeneity of Organic-Rich Sediments in the Rifle Aquifer, CO:

Impact on Uranium Biogeochemistry. Environmental Science & Technology 50, 46–53. https://doi.org/10.1021/acs.est.5b03208

Jones, B., Turki, A., 1997. Distribution and speciation of heavy metals in surficial sediments from the Tees Estuary, north-east England. Marine Pollution Bulletin 34, 768–779. https://doi.org/10.1016/S0025-326X(97)00047-7

Jouanneau, J.M., Latouche, C., Pautrizel, F., 1983. Analyse critique des extractions sequentielles a travers l'etude de quelques constituants des residus d'attaque critical analysis of sequential extractions through the study of several attack constituent residues. Environmental Technology Letters 4, 509–514. https://doi.org/10.1080/09593338309384240

Konhauser, K.O., Planavsky, N.J., Hardisty, D.S., Robbins, L.J., Warchola, T.J., Haugaard, R., Lalonde, S.V., Partin, C.A., Oonk, P.B.H., Tsikos, H., Lyons, T.W., Bekker, A., Johnson, C.M., 2017. Iron formations: A global record of Neoarchaean to Palaeoproterozoic environmental history. Earth-Science Reviews 172, 140–177. https://doi.org/10.1016/j.earscirev.2017.06.012

Koukina, S.E., Lobus, N.V., Peresypkin, V.I., Dara, O.M., Smurov, A.V., 2017. Abundance, distribution and bioavailability of major and trace elements in surface sediments from the Cai River estuary and Nha Trang Bay (South China Sea, Vietnam). Estuarine, Coastal and Shelf Science 198, 450–460. https://doi.org/10.1016/j.ecss.2016.03.005

Ku, T.C.W., Walter, L.M., 2003. Syndepositional formation of Fe-rich clays in tropical shelf sediments, San Blas Archipelago, Panama. Chemical Geology 197, 197–213. https://doi.org/10.1016/S0009-2541(02)00363-7

1057 Kumar, N., Lezama Pacheco, J., Noël, V., Dublet, G., Brown, G.E., 2018. Sulfidation
1058 mechanisms of Fe(III)-(oxyhydr)oxide nanoparticles: a spectroscopic study.
1059 Environmental Science: Nano 5, 1012–1026. https://doi.org/10.1039/C7EN01109A

1060 Lakshtanov, L.Z., Stipp, S.L.S., 2007. Experimental study of nickel(II) interaction with
1061 calcite: Adsorption and coprecipitation. Geochimica et Cosmochimica Acta 71, 3686–
1062 3697. https://doi.org/10.1016/j.gca.2007.04.006

1063 Lavigne, F. and Sahal, A., 2001. La réalité des risques majeurs en Nouvelle-Calédonie,
1064 Risques majeurs et institutions en Nouvelle-Calédonie, Cheroux B. and Faberon J.-Y.
1065 Eds, Presses Universitaires d'Aix-Marseille, pp 33-50.

1066 Le Pape, P., Blanchard, M., Brest, J., Boulliard, J.-C., Ikogou, M., Stetten, L., Wang, S.,
1067 Landrot, G., Morin, G., 2017. Arsenic Incorporation in Pyrite at Ambient Temperature
1068 at Both Tetrahedral S^{-I} and Octahedral Fe^{II} Sites: Evidence from EXAFS–DFT
1069 Analysis. Environmental Science & Technology 51, 150–158.
1070 https://doi.org/10.1021/acs.est.6b03502

1071 Lewis, M., Pryor, R., Wilking, L., 2011. Fate and effects of anthropogenic chemicals in
1072 mangrove ecosystems: A review. Environmental Pollution 159, 2328–2346.
1073 https://doi.org/10.1016/j.envpol.2011.04.027

1074 Li, Y.-L., Vali, H., Yang, J., Phelps, T.J., Zhang, C.L., 2006. Reduction of Iron Oxides
1075 Enhanced by a Sulfate-Reducing Bacterium and Biogenic H_2S. Geomicrobiology
1076 Journal 23, 103–117. https://doi.org/10.1080/01490450500533965

1077 López-Sánchez, J.F., Rubio, R., Samitier, C., Rauret, G., 1996. Trace metal partitioning in
1078 marine sediments and sludges deposited off the coast of Barcelona (Spain). Water
1079 Research 30, 153–159. https://doi.org/10.1016/0043-1354(95)00129-9

1080 Lovley, D.R., Chapelle, F.H. 1995. Deep subsurface microbial processes. Reviews of

1081 Geophysics, 33, 365-381. https://doi.org/10.1029/95RG01305

1082 Luther, G.W., Kostka, J.E., Church, T.M., Sulzberger, B., Stumm, W., 1992. Seasonal iron
1083 cycling in the salt-marsh sedimentary environment: the importance of ligand
1084 complexes with Fe(II) and Fe(III) in the dissolution of Fe(III) minerals and pyrite,
1085 respectively. Marine Chemistry 40, 81–103. https://doi.org/10.1016/0304-
1086 4203(92)90049-G

1087 Luther, G.W., 1987. Pyrite oxidation and reduction: Molecular orbital theory considerations.
1088 Geochimica et Cosmochimica Acta 51, 3193–3199. https://doi.org/10.1016/0016-
1089 7037(87)90127-X

1090 Magallanes-Ordóñez, V.R., Marmolejo-Rodríguez, A.J., Rodríguez-Figueroa, G.M., Sánchez-
1091 González, A., Aguíñiga-García, S., Arreguín-Sánchez, F., Zetina-Rejón, M., Tripp-
1092 Valdez, A., Romo-Ríos, J.A., 2015. Characterization of lithogenic and biogenic zones
1093 and natural enrichment of nickel in sediments of the Terminos Lagoon, Campeche,
1094 Mexico. Estuarine, Coastal and Shelf Science 156, 116–123.
1095 https://doi.org/10.1016/j.ecss.2014.11.007

1096 Maillot F., Morin G., Wang Y., Bonnin D., Ildefonse P., Chaneac C. and Calas G. (2011)
1097 New insight into the structure of nanocrystalline ferrihydrite: EXAFS evidence for
1098 tetrahedrally coordinated iron (III). Geochim. Cosmochim. Acta 75(10), 2708– 2720.

1099 Malinowski E. R. (1991) Factor Analysis in Chemistry. John Wiley, New York.

1100 Malinowski, E.R., 1987. Theory of the distribution of error eigenvalues resulting from
1101 principal component analysis with applications to spectroscopic data. Journal of
1102 Chemometrics 1, 33–40. https://doi.org/10.1002/cem.1180010106

1103 Malinowski E. R. (1978) Theory of error for target factor analysis with applications to mass
1104 spectrometry and nuclear magnetic resonance spectrometry. Anal. Chim. Acta 103,
1105 339–354. https://doi.org/10.1016/S0003-2670(01)83099-3

1106 Marchand, C., Fernandez, J.-M., Moreton, B., 2016. Trace metal geochemistry in mangrove
1107 sediments and their transfer to mangrove plants (New Caledonia). Science of The
1108 Total Environment 562, 216–227. https://doi.org/10.1016/j.scitotenv.2016.03.206

1109 Marchand, C., Fernandez, J.-M., Moreton, B., Landi, L., Lallier-Vergès, E., Baltzer, F., 2012.
1110 The partitioning of transitional metals (Fe, Mn, Ni, Cr) in mangrove sediments
1111 downstream of a ferralitized ultramafic watershed (New Caledonia). Chemical
1112 Geology 300-301, 70–80. https://doi.org/10.1016/j.chemgeo.2012.01.018

1113 Mejri, W., Ben Salah, I., Tlili, M.M., 2015. Speciation of Fe(II) and Fe(III) effect on $CaCO_3$
1114 crystallization: Speciation of Fe(II) and Fe(III) effect on $CaCO_3$ crystallization.
1115 Crystal Research and Technology 50, 236–243.
1116 https://doi.org/10.1002/crat.201400444

1117 Mettler, S., Wolthers, M., Charlet, L., Gunten, U. von, 2009. Sorption and catalytic oxidation
1118 of Fe(II) at the surface of calcite. Geochimica et Cosmochimica Acta 73, 1826–1840.
1119 https://doi.org/10.1016/j.gca.2009.01.003

1120 Minghelli-Roman, A., Dupouy, C. 2013. influence of water column chlorophyll concentration
1121 on bathymetric estimations in the lagoon of New Caledonia, using several MERIS
1122 images. IEEE Journal of Selected Topics in Applied Earth Observations and Remote
1123 Sensing, 6, 739-745. https://doi.org/10.1109/2239260

1124 Morad, S., Al-Ramadan, K., Ketzer, J.M., De Ros, L.F., 2010. The impact of diagenesis on
1125 the heterogeneity of sandstone reservoirs: A review of the role of depositional facies

1126 and sequence stratigraphy. AAPG Bulletin 94, 1267–1309.
1127 https://doi.org/10.1306/04211009178

1128 Morillo, J., Usero, J., Gracia, I., 2004. Heavy metal distribution in marine sediments from the
1129 southwest coast of Spain. Chemosphere 55, 431–442.
1130 https://doi.org/10.1016/j.chemosphere.2003.10.047

1131 Morin, G., Noël, V., Menguy, N., Brest, J., Baptiste, B., Tharaud, M., Ona-Nguema, G.,
1132 Ikogou, M., Viollier, E., Juillot, F., 2017. Nickel accelerates pyrite nucleation at
1133 ambient temperature. Geochemical Perspectives Letters 6–11.
1134 https://doi.org/10.7185/geochemlet.1738

1135 Morrison, R.J., Peshut, P.J., Lasorsa, B.K., 2010. Elemental composition and mineralogical
1136 characteristics of coastal marine sediments of Tutuila, American Samoa. Marine
1137 Pollution Bulletin 60, 925–930. https://doi.org/10.1016/j.marpolbul.2010.04.006

1138 Morse, J.W., Millero, F.J., Cornwell, J.C., Rickard, D., 1987. The chemistry of the hydrogen
1139 sulfide and iron sulfide systems in natural waters. Earth Science reviews, 24, 1-42.
1140 https://doi.org/10.1016/0012-8252(87)90046-8

1141 Morse, J.W., Luther Iii, G.W., 1999. Chemical influences on trace metal-sulfide interactions
1142 in anoxic sediments. Geochimica et Cosmochimica Acta 63, 3373–3378.
1143 https://doi.org/10.1016/S0016-7037(99)00258-6

1144 Morse, J.W., Wang, Q., 1997. Pyrite formation under conditions approximating those in
1145 anoxic sediments: II. Influence of precursor iron minerals and organic matter. Marine
1146 Chemistry 57, 187–193. https://doi.org/10.1016/S0304-4203(97)00050-9

1147 Morse, J.W., Millero, F.J., Cornwell, J. C., and Rickard, D. 1987. Chemistry of the hydrogen
1148 sulfide and iron sulfide systems in natural. Earth-Science Reviews, 1-42.
1149 https://doi.org/10.1016/0012-8252(87)90046-8

1150 Neretin, L.N., Böttcher, M.E., Jørgensen, B.B., Volkov, I.I., Lüschen, H., Hilgenfeldt, K.,
1151 2004. Pyritization processes and greigite formation in the advancing sulfidization front
1152 in the upper Pleistocene sediments of the Black Sea. Geochimica et Cosmochimica
1153 Acta 68, 2081–2093. https://doi.org/10.1016/S0016-7037(03)00450-2

1154 Neumann, T., Scholz, F., Kramar, U., Ostermaier, M., Rausch, N., Berner, Z., 2013. Arsenic
1155 in framboidal pyrite from recent sediments of a shallow water lagoon of the Baltic
1156 Sea. Sedimentology n/a-n/a. https://doi.org/10.1111/sed.12031

1157 Neumann, T., Rausch, N., Leipe, T., Dellwig, O., Berner, Z., Böttcher, M.E., 2005. Intense
1158 pyrite formation under low-sulfate conditions in the Achterwasser lagoon, SW Baltic
1159 Sea. Geochimica et Cosmochimica Acta 69, 3619–3630.
1160 https://doi.org/10.1016/j.gca.2005.02.034

1161 Nirel, P.M.V., Morel, F.M.M., 1990. Pitfalls of sequential extractions. Water Research 24,
1162 1055–1056. https://doi.org/10.1016/0043-1354(90)90129-T

1163 Noël, V., Juillot, F., Morin, G., Marchand, C., Ona-Nguema, G., Viollier, E., Prévot, F.,
1164 Dublet, G., Maillot, F., Delbes, L., Marakovic, G., Bargar, J.R., Brown, G.E., 2017.
1165 Oxidation of Ni-Rich Mangrove Sediments after Isolation from the Sea (Dumbea Bay,
1166 New Caledonia): Fe and Ni Behavior and Environmental Implications. ACS Earth and
1167 Space Chemistry 1, 455–464. https://doi.org/10.1021/acsearthspacechem.7b00005

1168 Noël, V., Morin, G., Juillot, F., Marchand, C., Brest, J., Bargar, J.R., Muñoz, M., Marakovic,
1169 G., Ardo, S., Brown, G.E., 2015. Ni cycling in mangrove sediments from New
1170 Caledonia. Geochimica et Cosmochimica Acta 169, 82–98.
1171 https://doi.org/10.1016/j.gca.2015.07.024

1172 Noël, V., Marchand, C., Juillot, F., Ona-Nguema, G., Viollier, E., Marakovic, G., Olivi, L.,
1173 Delbes, L., Gelebart, F., Morin, G., 2014. EXAFS analysis of iron cycling in

1174 mangrove sediments downstream a lateritized ultramafic watershed (Vavouto Bay,
1175 New Caledonia). Geochimica et Cosmochimica Acta 136, 211–228.
1176 https://doi.org/10.1016/j.gca.2014.03.019

1177 Oliveira, S.M.B. de, Partiti, C.S. de M., Enzweiler, J., 2001. Ochreous laterite: a nickel ore
1178 from Punta Gorda, Cuba. Journal of South American Earth Sciences 14, 307–317.
1179 https://doi.org/10.1016/S0895-9811(01)00026-8

1180 Ouillon, S., Douillet, P., Lefebvre, J.P., Le Gendre, R., Jouon, A., Bonneton, P., Fernandez,
1181 J.M., Chevillon, C., Magand, O., Lefèvre, J., Le Hir, P., Laganier, R., Dumas, F.,
1182 Marchesiello, P., Bel Madani, A., Andréfouët, S., Panché, J.Y., Fichez, R., 2010.
1183 Circulation and suspended sediment transport in a coral reef lagoon: the southwest lagoon
1184 of New Caledonia. Marine Pollution Bulletin, 61, 269–296.
1185 https://doi.org/10.1016/j.marpolbul.2010.06.023

1186 Oze, C., Bird, D.K., Fendorf, S., 2007. Genesis of hexavalent chromium from natural sources
1187 in soil and groundwater. Proceedings of the National Academy of Sciences 104, 6544–
1188 6549. https://doi.org/10.1073/pnas.0701085104

1189 Pacifico, R., Adamo, P., Cremisini, C., Spaziani, F., Ferrara, L., 2007. A geochemical
1190 analytical approach for the evaluation of heavy metal distribution in lagoon sediments.
1191 Journal of Soils and Sediments 7, 313–325. https://doi.org/10.1065/jss2007.06.231

1192 Passier, H. F., Middelburg, J. J., van Os, B. J. H., de Lange, G. J., 1996. Diagenetic
1193 pyritization under eastern Mediterranean sapropels caused by downward sulphide
1194 diffusion. Geochimica et Cosmochimica Acta 60, 5, 751–763.
1195 https://doi.org/10.1016/0016-7037(95)00419-X

1196 Raous, S., Echevarria, G., Sterckeman, T., Hanna, K., Thomas, F., Martins, E.S., Becquer, T.,
1197 2013. Potentially toxic metals in ultramafic mining materials: Identification of the

1198 main bearing and reactive phases. Geoderma 192, 111–119.
1199 https://doi.org/10.1016/j.geoderma.2012.08.017

1200 Rapin, F., Tessier, A., Campbell, P.G.C., Carignan, R., 1986. Potential artifacts in the
1201 determination of metal partitioning in sediments by a sequential extraction procedure.
1202 Environmental Science & Technology 20, 836–840.
1203 https://doi.org/10.1021/es00150a014

1204 Rasmussen, B., Muhling, J.R., Suvorova, A., Krapež, B., 2017. Greenalite precipitation
1205 linked to the deposition of banded iron formations downslope from a late Archean
1206 carbonate platform. Precambrian Research 290, 49–62.
1207 https://doi.org/10.1016/j.precamres.2016.12.005

1208 Rasmussen, B., Muhling, J.R., Suvorova, A., Krapež, B., 2016. Dust to dust: Evidence for the
1209 formation of "primary" hematite dust in banded iron formations via oxidation of iron
1210 silicate nanoparticles. Precambrian Research 284, 49–63.
1211 https://doi.org/10.1016/j.precamres.2016.07.003

1212 Rasmussen, B., Krapež, B., Muhling, J.R., Suvorova, A., 2015. Precipitation of iron silicate
1213 nanoparticles in early Precambrian oceans marks Earth's first iron age. Geology 43,
1214 303–306. https://doi.org/10.1130/G36309.1

1215 Rasmussen, B., Krape, B., Muhling, J.R., 2014a. Hematite replacement of iron-bearing
1216 precursor sediments in the 3.46-b.y.-old Marble Bar Chert, Pilbara craton, Australia.
1217 Geological Society of America Bulletin 126, 1245–1258.
1218 https://doi.org/10.1130/B31049.1

1219 Rasmussen, B., Krapez, B., Meier, D.B., 2014b. Replacement origin for hematite in 2.5 Ga
1220 banded iron formation: Evidence for postdepositional oxidation of iron-bearing

1221 minerals. Geological Society of America Bulletin 126, 438–446.
1222 https://doi.org/10.1130/B30944.1

1223 Ratié, G., Garnier, J., Calmels, D., Vantelon, D., Guimarães, E., Monvoisin, G., Nouet, J.,
1224 Ponzevera, E., Quantin, C., 2018. Nickel distribution and isotopic fractionation in a
1225 Brazilian lateritic regolith: Coupling Ni isotopes and Ni K-edge XANES. Geochimica
1226 et Cosmochimica Acta 230, 137–154. https://doi.org/10.1016/j.gca.2018.03.026

1227 Ravel B. and Newville M. (2005) ATHENA, ARTEMIS, HEPHAESTUS: data analysis for
1228 X-ray absorption spec- troscopy using IFEFFIT. J. Synchrotron Rad. 12, 537–541.
1229 https://doi.org/10.1107/S0909049505012719

1230 Retallack, G.J., 2010. Lateritization and bauxitization events. Economic Geology 105, 655–
1231 667. https://doi.org/10.2113/gsecongeo.105.3.655

1232 Rickard, D., Luther, G.W., 2007. Chemistry of Iron Sulfides. Chemical Reviews 107, 514–
1233 562. https://doi.org/10.1021/cr0503658

1234 Rickard, D., Morse, J.W., 2005. Acid volatile sulfide (AVS). Marine Chemistry 97, 141–197.
1235 https://doi.org/10.1016/j.marchem.2005.08.004

1236 Rickard, D., Luther, G.W., 1997. Kinetics of pyrite formation by the H2S oxidation of iron(II)
1237 monosulfide in aqueous solutions between 25 and 125°C: The mechanism.
1238 Geochimica et Comoschimica Acta 61, 135-147. https://doi.org/10.11016/S0016-
1239 7037(96)00321-3

1240 Roberts, A.P., Turner, G.M., 1993. Diagenetic formation of ferrimagnetic iron sulfide
1241 minerals in rapidly deposited marine sediments, South Island, New Zealand. Earth and
1242 Planetary Science Letters 115, 257–273. https://doi.org/10.1016/0012-
1243 821X(93)90226-Y

1244 Sabadini-Santos, E., Senez, T.M., Silva, T.S., Moreira, M.R., Mendonça-Filho, J.G., Santelli,
1245 R.E., Crapez, M.A.C., 2014. Organic matter and pyritization relationship in recent
1246 sediments from a tropical and eutrophic bay. Marine Pollution Bulletin 89, 220–228.
1247 https://doi.org/10.1016/j.marpolbul.2014.09.055

1248 Saravanan, P., Pradhap, D., Krishnakumar, S., Silva, J.D., Vidyasakar, A., Sackaria, M.,
1249 Godson, P.S., Arumugam, K., Magesh, N.S., 2018. A baseline study on trace element
1250 based sediment pollution and potential ecological risk of reef sediments of Musal,
1251 Manoli and Manoli putti Islands, Gulf of Mannar, India. Marine Pollution Bulletin
1252 133, 117–123. https://doi.org/10.1016/j.marpolbul.2018.05.024

1253 Scholz, F., Neumann, T., 2007. Trace element diagenesis in pyrite-rich sediments of the
1254 Achterwasser lagoon, SW Baltic Sea. Marine Chemistry 107, 516–532.
1255 https://doi.org/10.1016/j.marchem.2007.08.005

1256 Sevin, B., Ricordel-Prognon, C., Quesnel, F., Cluzel, D., Lesimple, S., Maurizot, P., 2012.
1257 First palaeomagnetic dating of ferricrete in New Caledonia: new insight on the
1258 morphogenesis and palaeoweathering of 'Grande Terre': First palaeomagnetic dating
1259 of ferricrete in New Caledonia. Terra Nova 24, 77–85. https://doi.org/10.1111/j.1365-
1260 3121.2011.01041.x

1261 Snyder R.L. and Bish D.L. (1989) Quantitative analysis, in Modern powder diffraction,
1262 reviews in mineralogy, Vol 20., D.L. Bish and J.E. Post Eds, Mineralogical Society of
1263 America, pp 101-144.

1264 Stetten, L., Mangeret, A., Brest, J., Seder-Colomina, M., Le Pape, P., Ikogou, M., Zeyen, N.,
1265 Thouvenot, A., Julien, A., Alcalde, G., Reyss, J.L., Bombled, B., Rabouille, C., Olivi,
1266 L., Proux, O., Cazala, C., Morin, G., 2018. Geochemical control on the reduction of

1267 U(VI) to mononuclear U(IV) species in lacustrine sediments. Geochimica et
1268 Cosmochimica Acta 222, 171–186. https://doi.org/10.1016/j.gca.2017.10.026

1269 Tardy, Y. (1997) : Petrology of Laterites and Tropical Soils. 419 p. ISBN 978-9054- 106784

1270 Taylor, K.G., Macquaker, J.H.S., 2011. Iron Minerals in Marine Sediments Record Chemical
1271 Environments. Elements 7, 113–118. https://doi.org/10.2113/gselements.7.2.113

1272 Torreton, J.-P., Rochelle-Newall, E., Jouon, A., Faure, V., Jacquet, S., Douillet, P., 2007.
1273 Correspondence between the distribution of hydrodynamic time parameters and the
1274 distribution of biological and chemical variables in a semi-enclosed coral reef lagoon.
1275 Estuarine, Coastal and Shelf Science, 74, 766–776.
1276 https://doi.org/10.1016/j.ecss.2007.05.018

1277 Torreton, J.P., Rochelle-Newall, E., Pringault, O., Jacquet, S., Faure., V., Briand., E., 2010.
1278 Variability of primary and bacterial production in a coral reef lagoon (New Caledonia).
1279 Marine Pollution Bulletin, 61, 335–348. https://doi.org/10.1016/j.marpolbul.2010.06.019

1280 Vincent, B., Jourand, P., Juillot, F., Ducousso, M., Galiana, A., 2018. Biological *in situ*
1281 nitrogen fixation by an Acacia species reaches optimal rates on extremely contrasted
1282 soils. European Journal of Soil Biology 86, 52–62.
1283 https://doi.org/10.1016/j.ejsobi.2018.03.003

1284 Wang, B., Zhao, F., Zhang, H., Fang, Y., Zheng, D., 2012. WIDESPREAD PYRITIZATION
1285 OF INSECTS IN THE EARLY CRETACEOUS JEHOL BIOTA. PALAIOS 27, 707–
1286 711. https://doi.org/10.2110/palo.2012.p12-029r

1287 Wang, Q., Morse, J.W., 1996. Pyrite formation under conditions approximating those in
1288 anoxic sediments I. Pathway and morphology. Marine Chemistry 52, 99–121.
1289 https://doi.org/10.1016/0304-4203(95)00082-8

1290 Wattelez G., Dupouy C., Lefevre J, Ouillon S ;, Fernandez J.M. and Juillot F., 2016.
1291 Application of the support vector regression method for turbidity assessment with
1292 MODIS on a shallow Coral reef lagoon (Voh-Kone_pouembout, New Caledonia).
1293 Water, 9, 137. https://doi:10.3390/w9100737

1294 Webb S. M. (2005) SIXpack: a graphical user interface for XAS analysis using IFEFFIT.
1295 Phys. Scripta T115, 1011.

1296 Wilkin, R.T., Beak, D.G., 2017. Uptake of nickel by synthetic mackinawite. Chemical
1297 Geology 462, 15–29. https://doi.org/10.1016/j.chemgeo.2017.04.023

1298 Wilkin, R.T., Barnes, H.L., 1997. Formation processes of framboidal pyrite. Geochimica et
1299 Cosmochimica Acta 61, 323-339. https://doi.org/10.1016/S0016-7037(96)00320-1

1300 Wilson, J., Savage, D., Cuadros, J., Shibata, M., Ragnarsdottir, K.V., 2006. The effect of iron
1301 on montmorillonite stability. (I) Background and thermodynamic considerations.
1302 Geochimica et Cosmochimica Acta 70, 306–322.
1303 https://doi.org/10.1016/j.gca.2005.10.003

1304 Wu, T., Griffin, A.M., Gorski, C.A., Shelobolina, E.S., Xu, H., Kukkadapu, R.K., Roden,
1305 E.E., 2017. Interactions Between Fe(III)-oxides and Fe(III)-phyllosilicates During
1306 Microbial Reduction 2: Natural Subsurface Sediments. Geomicrobiology Journal 34,
1307 231–241. https://doi.org/10.1080/01490451.2016.1174758

1308 Yongue-Fouateu, R., Ghogomu, R.T., Penaye, J., Ekodeck, G.E., Stendal, H., Colin, F., 2006.
1309 Nickel and cobalt distribution in the laterites of the Lomié region, south-east
1310 Cameroon. Journal of African Earth Sciences 45, 33–47.
1311 https://doi.org/10.1016/j.jafrearsci.2006.01.003

Yuan, C., Shi, J., He, B., Liu, J., Liang, L., Jiang, G., 2004. Speciation of heavy metals in marine sediments from the East China Sea by ICP-MS with sequential extraction. Environment International 30, 769–783. https://doi.org/10.1016/j.envint.2004.01.001

Zonta, R., Botter, M., Cassin, D., Bellucci, L.G., Pini, R., Dominik, J., 2018. Sediment texture and metal contamination in the Venice Lagoon (Italy): A snapshot before the installation of the MOSE system. Estuarine, Coastal and Shelf Science 205, 131–151. https://doi.org/10.1016/j.ecss.2018.03.007

FIGURES CAPTION

Figure 1. Map of the studied area showing the sediment sampling stations in the Chasseloup (ST16), Vavouto (VE2, WR2 and LG2B) and Kataviti (KTV, KL1 and KL2) Bays displayed on a simplified geological map of the studied area. Topographic map data are from google.com and geological map are from Georep (2019).

Figure 2. Results of the combined PCA/HCPC analysis of the studied sediments. The left panel depicts the loading of the variables (*i.e*. concentrations of major and trace elements) on the PCA factors 1 and 2 and the right panel shows the four groups of sediments defined on the HCPC factor score.

Figure 3. Mineralogical composition of representative samples (at a depth of 8cm) from the seven stations, as determined by Rietveld refinement of the XRD patterns. Corresponding data are reported in Figures S8-10 and Table S3. The mineral species identified are albite (Ab), aragonite (Arg), calcite (Cal), chrysotile (Ctl), greenalite/berthierine (Gre/Ber), halite

(Hl), illite/mscuvoite (Ill/Ms), illite/mscuvoite/smectite (Ill/Ms/Sme), magnesian calcite (Cal-Mg), pyrite (Py) and quartz (Qtz).

Figure 4. TEM images and TEM-EDXS spectra of representative Ni-bearing clay minerals observed in the VE2 1-2 cm and 7.5-8.5 cm sediment samples from the Vavouto Bay. Atomic composition derived from TEM-EDXS analysis of the observed clay particles are displayed as plain triangles in a Si+Al, Mg, Fe ternary diagram, where ideal compositions of reference clay minerals are plotted as plain circles: chrysotile (green), talc (gray), greenalite (blue), berthierine (light-blue), nontronite (pink), montmorillonite (purple), glauconite (red) and odinite (light-gray). Compositions of additional clay particles are reported as open triangles with corresponding composition reported Table 2.

Figure 5. Speciation of S, Fe and Ni determined by LC-LSF analysis of S K-edge XANES and Fe and Ni K-edge EXAFS data for the 7.5-8.5 cm depth sample from the seven stations. LC-LSF analysis results of the whole sample set are reported in Figures S15, S18 and S23 and Tables S6, S8 and S11 for S, Fe and Ni, respectively.

TABLES CAPTION

Table 1. Mean concentrations of Total Organic Carbon (TOC), Total Organic Nitrogen (TON), Ca, K, Mg, Na, Si, Al, Fe and Ti (in wt%) and Cr, Mn, Co, Ni, Cu and Zn (in $mg.kg^{-1}$) in the studied lagoon sediments. For each station, the concentrations given correspond to an average along the whole sediment core. Uncertainties are estimated at ± 5% of the stated values.

Table 2. Semi-quantitative TEM-EDXS chemical composition (wt% oxides and atom%) of the chrysotile, greenalite, berthierine, glauconite and Fe-rich smectite observed in the VE2 1-2cm and 7.5-8.5cm sediment samples from the Vavouto Bay and plotted on the Si/Al, Mg, Fe ternary diagram in Figure 4. n.d.: not detected. Uncertainties are estimated at ± 10% of the stated values for wt% oxides.

Table
Click here to download Table: Merrot_STOTEN_2019_revised_Tables.docx

Nickel and iron partitioning between clay minerals, Fe-oxides and Fe-sulfides in lagoon sediments from New Caledonia

Pauline Merrot[a], Farid Juillot[a,b], Vincent Noël[c], Pierre Lefebvre[a], Jessica Brest[a], Nicolas Menguy[a], Jean-Michel Guigner[a], Marine Blondeau[a] , Eric Viollier[d], Jean-Michel Fernandez[e], Benjamin Moreton[e], John Bargar[c] and Guillaume Morin[a]

[a] *Institut de Minéralogie, de Physique des Matériaux et de Cosmochimie (IMPMC), UMR 7590 CNRS-SU-IRD-MNHN, Sorbonne Université, case 115, 4 place Jussieu, 75252 Paris Cedex 5, France*

[b] *Institut de Recherche pour le développement (IRD), UMR 206/UMR 7590 IMPMC, 98848 Nouméa, New Caledonia*

[c] *Stanford Synchrotron Radiation Lightsource, SLAC National Accelerator Laboratory, 2575 Sand Hill Road, MS 69, Menlo Park, CA 94025, USA*

[d] *Institut de Physique du Globe de Paris (IPGP), Sorbonne Paris Cité, Univ Paris Diderot, CNRS, F-75005 Paris, France*

[e] *Analytical Environmental Laboratory (AEL), 98800 Nouméa, New Caledonia*

TABLES

Table 1. Mean concentrations of Total Organic Carbon (TOC), Total Organic Nitrogen (TON), Ca, K, Mg, Na, Si, Al, Fe and Ti (in wt%) and Cr, Mn, Co, Ni, Cu and Zn (in $mg.kg^{-1}$) in the studied lagoon sediments. For each station, the concentrations given correspond to an average along the whole sediment core. Uncertainties are estimated at ± 5% of the stated values.

Station	TOC	TON	Ca	K	Mg	Na	Si	Al	Fe	Ti	Cr	Mn	Co	Ni	Cu	Zn
KTV	3.34	0.14	1.86	0.74	2.26	2.80	28.38	5.47	7.10	0.42	2879	547	85	1505	38	86
sd	*0.39*	*0.02*	*0.62*	*0.09*	*0.10*	*0.29*	*0.98*	*0.30*	*0.57*	*0.02*	*378*	*42*	*46*	*391*	*03*	*06*
KL1	2.42	0.13	5.90	0.93	1.89	2.14	25.70	5.80	5.59	0.46	570	482	54	553	34	51
sd	*0.31*	*0.01*	*0.48*	*0.05*	*0.04*	*0.34*	*0.53*	*0.20*	*0.24*	*0.02*	*20*	*28*	*17*	*42*	*11*	*04*
KL2	1.89	0.14	13.02	0.78	1.90	2.28	18.15	4.30	3.75	0.33	334	456	45	390	31	40
sd	*0.38*	*0.01*	*0.46*	*0.05*	*0.06*	*0.49*	*0.59*	*0.19*	*0.18*	*0.01*	*10*	*31*	*28*	*23*	*03*	*05*
VE2	2.51	0.12	1.40	0.64	2.23	2.27	32.94	5.14	4.86	0.39	1512	446	66	905	27	65
sd	*0.38*	*0.02*	*0.25*	*0.12*	*0.34*	*0.42*	*0.49*	*0.79*	*0.88*	*0.06*	*260*	*109*	*10*	*157*	*06*	*12*
WR2	1.44	0.10	19.01	0.43	1.89	1.67	15.98	3.01	3.30	0.22	779	376	43	633	23	34
sd	*0.04*	*0.01*	*0.49*	*0.01*	*0.03*	*0.17*	*0.39*	*0.06*	*0.06*	*0.01*	*37*	*17*	*01*	*20*	*02*	*06*
LG2B	1.08	0.07	29.57	0.31	1.63	1.08	8.26	1.76	2.67	0.13	278	335	29	327	17	22
sd	*0.09*	*0.01*	*0.97*	*0.02*	*0.04*	*0.15*	*0.75*	*0.11*	*0.12*	*0.01*	*24*	*20*	*14*	*26*	*03*	*04*
ST16	4.39	0.20	1.01	1.15	1.67	2.33	32.47	6.18	4.49	0.50	517	370	45	255	26	63
sd	*0.49*	*0.03*	*0.13*	*0.13*	*0.07*	*0.25*	*1.02*	*0.42*	*0.18*	*0.02*	*112*	*22*	*42*	*30*	*04*	*11*

Table 2. Semi-quantitative TEM-EDXS chemical composition (wt% oxides and atom%) of the chrysotile, greenalite, berthierine, glauconite and Fe-rich smectite observed in the VE2 1-2cm and 7.5-8.5cm sediment samples from the Vavouto Bay and plotted on the Si/Al, Mg, Fe ternary diagram in Figure 4. n.d.: not detected. Uncertainties are estimated at ± 10% of the stated values for wt% oxides.

	CHRYSOTILE					GREENALITE			BERTHIERINE				GLAUCONITE		NONT*
Wt% (oxides)	1	2	3	4	5	1	2	3	1	2	3	4	1	2	1
MgO	36.0	34.5	32.3	37.0	37.1	2.9	3.1	2.5	2.5	2.6	1.0	2.5	7.3	5.1	2.6
FeO	11.9	13.2	12.4	7.8	7.2	53.5	52.6	54.5	46.6	46.4	41.8	41.9	19.5	30.5	36.6
Al_2O_3	0.6	1.4	2.3	2.2	2.6	6.2	6.1	4.7	17.8	17.4	2.3	6.2	18.5	18.4	16.9
SiO_2	50.7	49.5	51.6	50.3	50.6	25.1	25.3	24.9	28.8	28.8	49.2	42.3	48.8	40.0	39.2
NiO	n.d.	0.1	0.2	0.1	0.0	6.2	6.8	7.3	1.2	1.2	0.8	0.9	n.d.	n.d.	0.8
$C_{r2}O_3$	0.4	0.5	0.8	0.8	0.7	1.0	1.0	0.8	1.7	1.6	1.2	1.2	0.6	1.2	1.1
Atom%	1	2	3	4	5	1	2	3	1	2	3	4	1	2	1
Mg	2.26	2.19	2.02	2.31	2.31	0.26	0.28	0.23	0.20	0.20	0.08	0.19	0.73	0.54	0.27
Fe	0.42	0.47	0.44	0.27	0.25	2.69	2.64	2.80	2.03	2.03	1.73	1.80	0.98	1.62	1.95
Al	0.03	0.07	0.11	0.11	0.13	0.44	0.43	0.34	1.09	1.07	0.13	0.38	1.46	1.53	1.41
Si	2.13	2.10	2.16	2.11	2.11	1.51	1.52	1.52	1.50	1.51	2.44	2.17	3.28	2.82	2.77
Ni	0.00	0.00	0.01	0.00	0.00	0.30	0.33	0.36	0.05	0.05	0.03	0.04	0.00	0.00	0.02
Cr	0.01	0.02	0.03	0.03	0.02	0.05	0.05	0.04	0.07	0.07	0.05	0.05	0.03	0.07	0.05
∑ cations **	2.72	2.75	2.60	2.72	2.71	3.25	3.24	3.29	2.93	2.93	2.47	2.62	2.49	2.57	2.47

* Nontronite

** Based on $O_5(OH)_4$ for chrysotile, greenalite and berthierine and on $O_{10}(OH)_2$ for glauconite and smectite.

** All Al as Al_{oct} for chrysotile, Al_{oct} = atom%(Al) - [2 - atom%(Si)] for greenalite and berthierine and Al_{oct} = atom%(Al) - [4 - atom%(Si)] for glauconite and smectite.

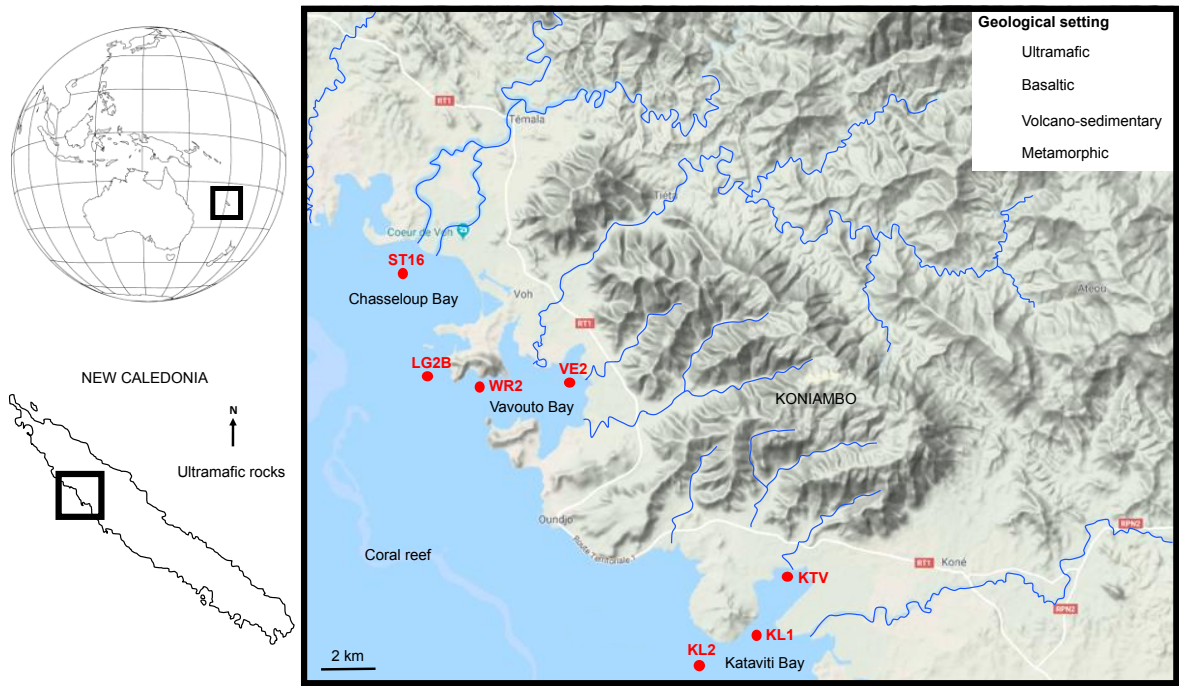

Figure 1. Map of the studied area showing the sediment sampling stations in the Chasseloup (ST16), Vavouto (VE2, WR2 and LG2B) and Kataviti (KTV, KL1 and KL2) Bays displayed on a simplified geological map of the studied area. Topographic map data are from google.com and geological map are from Georep (2019).

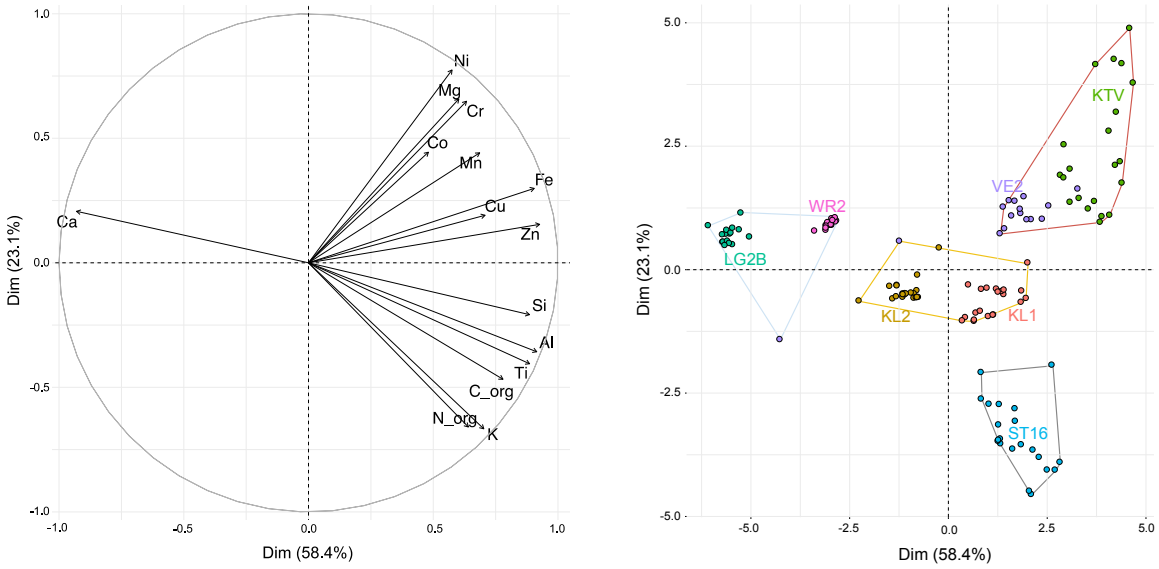

Figure 2. Results of the combined PCA/HCPC analysis of the studied sediments. The left panel depicts the loading of the variables (*i.e*. concentrations of major and trace elements) on the PCA factors 1 and 2 and the right panel shows the four groups of sediments defined on the HCPC factor score.

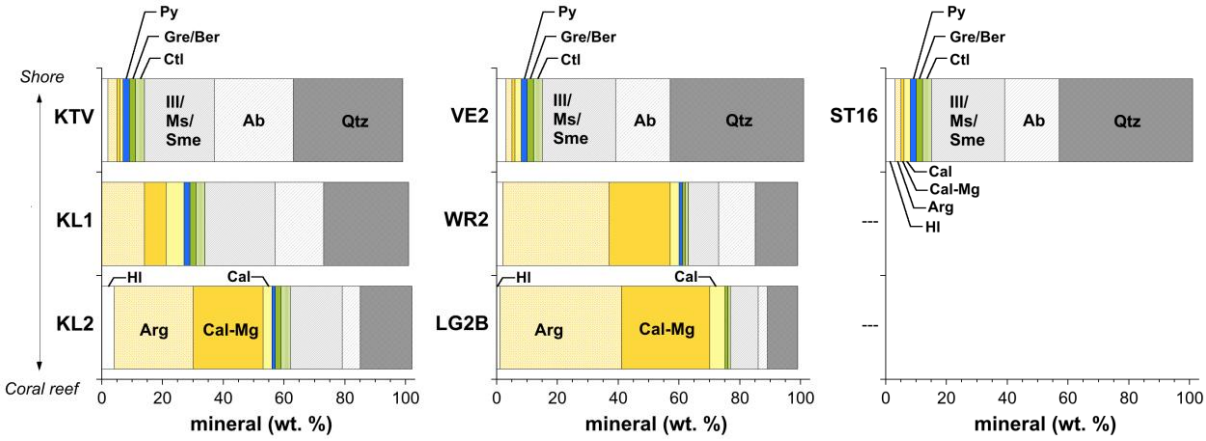

Figure 3. Mineralogical composition of representative samples (at a depth of 8cm) from the seven stations, as determined by Rietveld refinement of the XRD patterns. Corresponding data are reported in Figures S8-10 and Table S3. The mineral species identified are albite (Ab), aragonite (Arg), calcite (Cal), chrysotile (Ctl), greenalite/berthierine (Gre/Ber), halite (Hl), illite/mscuvoite (Ill/Ms), illite/mscuvoite/smectite (Ill/Ms/Sme), magnesian calcite (Cal-Mg), pyrite (Py) and quartz (Qtz).

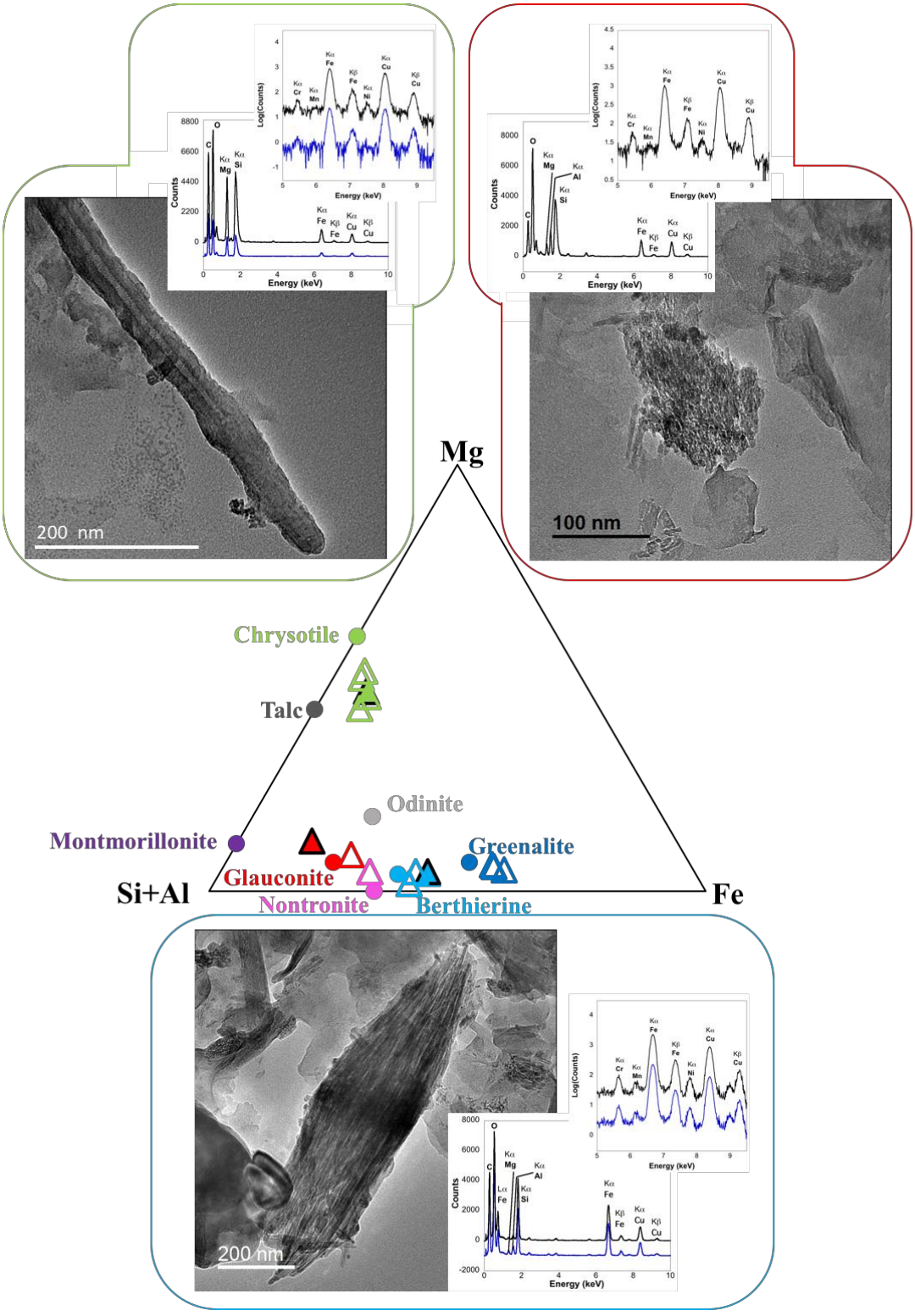

Figure 4. TEM images and TEM-EDXS spectra of representative Ni-bearing clay minerals observed in the VE2 1-2 cm and 7.5-8.5 cm sediment samples from the Vavouto Bay. Atomic composition derived from TEM-EDXS analysis of the observed clay particles are displayed as plain triangles in a Si+Al, Mg, Fe ternary diagram, where ideal compositions of reference clay minerals are plotted as plain circles: chrysotile (green), talc (gray), greenalite (blue), berthierine (light-blue), nontronite (pink), montmorillonite (purple), glauconite (red) and odinite (light-gray). Compositions of additional clay particles are reported as open triangles with corresponding composition reported Table 2.

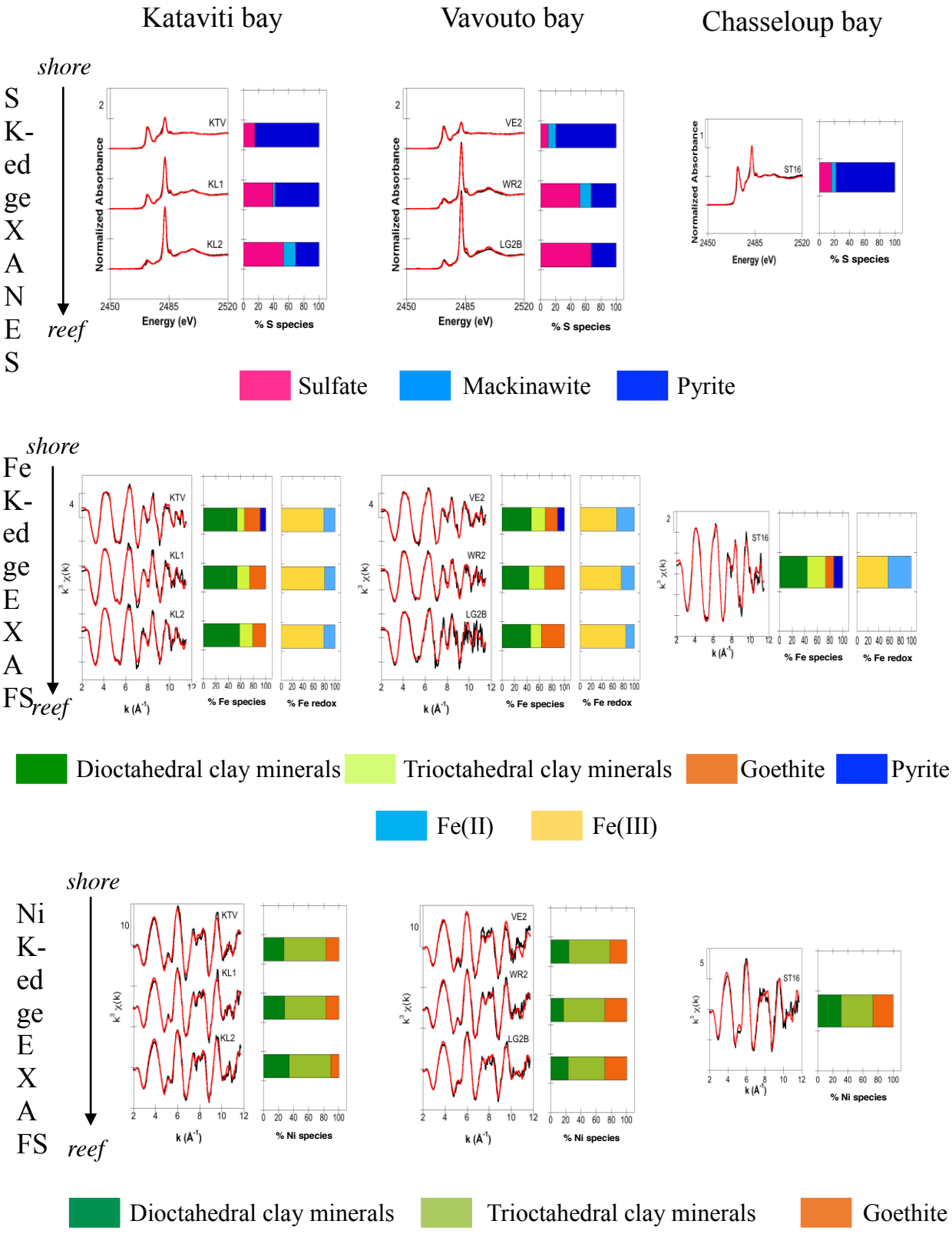

Figure 5. Speciation of S, Fe and Ni determined by LC-LSF analysis of S K-edge XANES and Fe and Ni K-edge EXAFS data for the 7.5-8.5 cm depth sample from the seven stations. LC-LSF analysis results of the whole sample set are reported in Figures S15, S18 and S23 and Tables S6, S8 and S11 for S, Fe and Ni, respectively.